TIME-DEPENDENT DENSITY FUNCTIONAL THEORY: HOW ACCURATE IS ALDA ?

BY JAN WERSCHNIK

A thesis submitted to the

Graduate School—New Brunswick

Rutgers, The State University of New Jersey

in partial fulfillment of the requirements

for the degree of

Master of Science

Graduate Program in Physics and Astronomy

Written under the direction of

Kieron Burke

and approved by

New Brunswick, New Jersey

October, 2001

ABSTRACT OF THE THESIS

Time-dependent density functional theory: How accurate is ALDA ?

by Jan Werschnik

Thesis Director: Kieron Burke

We calculate the time-evolution of the density for Hooke's atom, starting in the ground-state. We analyze the time-dependence via the spread of the density $\langle r^2 \rangle$ and evaluate its Fourier transform. The frequency contributions are explained and compared to an approximate calculation using the adiabatic local density approximation (ALDA). In the time domain we find a good agreement between our exact calculation and the ALDA for short times, but differences at larger times. The differences are caused by "missing" peaks in the ALDA spectrum.

Table of Contents

List of Tables

List of Figures

Chapter 1

Introduction

1.1 An introduction to ground-state DFT

Density functional theory (DFT) has become an important tool in electronic structure calculations. The interest in electronic structure calculations is very high, since the electronic structure determines most of of the chemical and physical properties of atoms, molecules and solids. This section is meant as a brief introduction to the basics of DFT. The issues of degenerate ground-states, fractional particle numbers and v-representability [1] are neglected in this introduction and also in the subsequent sections. Also, all electrons are spinless and atomic units are used throughout.
Within the Born-Oppenheimer approximation the Schrödinger equation of a many electron system looks like:

$$\begin{aligned} \hat{H}\Psi = \left\{\hat{T} + \hat{W} + \hat{V}_{ext}\right\}\Psi &= E\Psi \\ \left\{\sum_{i=1}^{N} -\frac{1}{2}\nabla_i^2 + \frac{1}{2}\sum_{i=1}^{N}\sum_{\substack{j=1 \\ j\neq i}}^{N} \frac{1}{|\mathbf{r}_i - \mathbf{r}_j|} + \sum_{i=1}^{N} v_{ext}(\mathbf{r}_i)\right\}\Psi &= E\Psi \end{aligned} \tag{1.1}$$

The Coulomb interaction term makes it impossible to solve the Schrödinger equation analytically ($N \geq 2$) (except for a few special cases) and even numerically the solution of this equation becomes very expensive.
With a density functional approach, we can in principle calculate any property of the system using the ground-state density n_0

$$n_0(\mathbf{r}) = N \int d\mathbf{r}_2 \ldots d\mathbf{r}_N \left|\Psi_0(\mathbf{r}, \mathbf{r}_2, \ldots, \mathbf{r}_N)\right|^2, \tag{1.2}$$

and a functional for the specific property. In DFT the knowledge of the many-electron wave-function itself is not necessary.

1.1.1 The Hohenberg-Kohn theorem

The birth of modern DFT goes back to 1964, when Hohenberg and Kohn [2] published their paper: "Inhomogeneous electron gas".

In their paper they were able to prove, that the surjective mappings from the external potential to the interacting ground-state and from the interacting ground-state to the ground-state density

$$v_{\text{ext}}(\mathbf{r}) \quad \mapsto \quad \Psi_0(\mathbf{r}_0, \ldots, \mathbf{r}_N) \tag{1.3}$$

$$\Psi_0(\mathbf{r}_0, \ldots, \mathbf{r}_N) \quad \mapsto \quad n_0(\mathbf{r}) \tag{1.4}$$

are injective and thus both of these mappings could be inverted. That means, there exists a one-to-one mapping from the ground-state density to the external potential v_{ext}: $v_{\text{ext}}(\mathbf{r}) \leftrightarrow n_0(\mathbf{r})$.

The paper gives three important statements:

1. The ground-state expectation value of an arbitrary observable $\hat{O}$ may be expressed as an unique functional of the ground-state density. In particular the ground-state energy

$$E_0[n_0] \quad = \quad \langle \Psi_0[n_0] | \hat{T} + \hat{W} + \hat{V}_{ext} | \Psi_0[n_0] \rangle \,, \tag{1.5}$$

   where $\Psi_0[n_0]$ is the ground-state wave-function with density $n_0(\mathbf{r})$, defined in (1.2). The expression indicates the functional dependence on the ground-state density $n_0(\mathbf{r})$.

2. Due to the Rayleigh-Ritz variational principle, the ground-state energy $E_0[n]$, can be determined by a minimization process, i.e.

$$\varepsilon_0 \quad = \quad E_0[n_0] = \min_n \; E_0[n] \tag{1.6}$$

$$\varepsilon_0 \quad < \quad E_0[n] \qquad \text{if} \qquad n \neq n_0 \tag{1.7}$$

3. If we rewrite (1.5) in the following way,

$$E_0[n_0] \quad = \quad \underbrace{\langle \Psi_0[n_0] | \hat{T} + \hat{W} | \Psi_0[n_0] \rangle}_{F_{HK}[n_0]} + \int d\mathbf{r} \; v_{\text{ext}}(\mathbf{r}) \, n_0(\mathbf{r}) \tag{1.8}$$

we see that the functional $F_{HK}[n_0]$ has a universal character. In other words it is the same for all electronic structure problems (atoms, molecules and solids). The difference between these systems is given by the external potential $v_{\text{ext}}(\mathbf{r})$.

Because the ground-state density determines the potential, and therefore the Hamiltonian, it determines in principle any property of the system, even excited states. In practice we are not any closer to the solution of our problem, since the paper does not give an answer on how to construct the functional $F_{HK}[n_0]$.

1.1.2 The Kohn-Sham system

Kohn and Sham [3] introduced a fictitious N particle system without particle-particle interaction and the crucial assumption that there exists a local potential $v_s(\mathbf{r})$, so that the density $n_s(\mathbf{r})$ *equals* the ground-state density of the interacting system $n_s(\mathbf{r}) = n_0(\mathbf{r})$. The Kohn-Sham orbitals of this non-interacting system solve

$$\left\{-\frac{1}{2}\nabla^2 + v_s[n_0](\mathbf{r})\right\}\phi_i(\mathbf{r}) = \epsilon_i\phi_i(\mathbf{r}) \tag{1.9}$$

$$n_0(\mathbf{r}) = n_s(\mathbf{r}) = \sum_{\text{N lowest eigenstates}} |\phi_i(\mathbf{r})|^2 \tag{1.10}$$

$$\Phi = \frac{1}{\sqrt{N!}} \det \{\phi_i(\mathbf{r}_k)\} \tag{1.11}$$

Now, we just need to know $v_s[n_0](\mathbf{r})$, find the eigenstates and eigenvalues of (1.9) and construct the ground-state density $n_0(\mathbf{r})$. The uncoupled equations (1.9) are much easier to solve then the interacting many-body Schrödinger equation (1.1) and are in principle exact, including correlation effects (unlike Hartree-Fock).

To find an expression for v_s we apply the knowledge from the Hohenberg-Kohn paper.

1. The first statement ensures that for a given density $v_s(\mathbf{r})$ is unique, thus it follows that the single-particle orbitals $|\phi_i[n_0]\rangle$ and the non-interacting kinetic energy $T_s[n_0]$ are unique functionals of the density $n_0(\mathbf{r})$.

   The ground-state energy of an interacting system may be written as a sum of four terms: the non-interacting kinetic energy $T_s[n_0]$, the external potential, the classical electrostatic energy, called the Hartree term $E_H[n_0]$ and the exchange correlation energy $E_{xc}[n_0]$, which describes what is left.

$$
\begin{aligned}
E_H[n_0] &= \frac{1}{2}\iint d\mathbf{r}d\mathbf{r}' \ \frac{n(\mathbf{r})n(\mathbf{r}')}{|\mathbf{r}-\mathbf{r}'|} && (1.12)\\
E_0[n_0] &= T_s[n] + \int d\mathbf{r} \ n_0(\mathbf{r})v_{\text{ext}}(\mathbf{r}) + E_H[n_0] + E_{xc}[n_0] && (1.13)\\
E_{xc}[n_0] &= F_{HK}[n_0] - T_s[n_0] - E_H[n_0] && (1.14)
\end{aligned}
$$

2. The statement about the variational character helps us to define $v_s[n_0](\mathbf{r})$ in a formal way. The variation of the ground-state energy around the minimum density $n_0(\mathbf{r})$ vanishes

$$
\begin{aligned}
\delta E_0 &= E_0[n_0+\delta n] - E_0[n_0] = 0 && (1.15)\\
\delta E_0 &= \delta T_s[n_0] + \int d\mathbf{r} \ \delta n(\mathbf{r}) \left[v_{ext}(\mathbf{r}) + \int d\mathbf{r}' \ \frac{n_0}{|\mathbf{r}_i - \mathbf{r}_j|} + v_{xc}[n_0](\mathbf{r}) \right], && (1.16)
\end{aligned}
$$

where

$$
v_{xc}[n_0](\mathbf{r}) = \left.\frac{\delta E_{xc}[n]}{\delta n(\mathbf{r})}\right|_{n_0} \tag{1.17}
$$

Using the fact that the single-particle orbitals of the Slater determinant $\Phi[n]$ satisfy the Schrödinger equation (1.9), one can show

$$
\delta T_s[n_0] = \delta\langle\Phi[n_0]|\hat{T}|\Phi[n_0]\rangle = -\int d\mathbf{r} \ v_s \delta n(\mathbf{r}) \tag{1.18}
$$

Inserting (1.18) in (1.16) we find v_s to be defined as

$$
v_s[n_0](\mathbf{r}) = v_{\text{ext}}(\mathbf{r}) + \int d\mathbf{r}' \ \frac{n_0(\mathbf{r}')}{|\mathbf{r}-\mathbf{r}'|} + v_{xc}[n_0](\mathbf{r}) \tag{1.19}
$$

where we recognize the second term on the right-hand-side is the classical Hartree potential, $v_H[n_0](\mathbf{r})$.

The solution of the Kohn Sham System (1.9) with $v_s[n_0](\mathbf{r})$, given in (1.19), is found via self consistent calculations. The scheme could look like this:

1. take $v_s^{(0)}(\mathbf{r})$=$v_{\text{ext}}(\mathbf{r})$

2. solve the one particle Schrödinger equation (1.9)

3. calculate the density from (1.10)

4. calculate $v_s[n](\mathbf{r})$ from the density using (1.19)

5. go to (2).

But one problem still remains: What are $E_{xc}[n]$ and $v_{xc}[n](\mathbf{r})$?

Until here the derivation was exact, there was no approximation made (the self consistency cycle would converge against the exact ground-state density). But since no one knows the universal $v_{xc}[n](\mathbf{r})$ so far, it is necessary to use approximate functionals. There are several approximations for these functionals available. The simplest one is called the Local Density Approximation (LDA), which is exact for the homogeneous electron gas. It turned out that this rather simple approximation yields very good results even for inhomogeneous systems due to exact conditions that the functionals satisfy [4]. It is still used today in many calculations in solid state physics. We discuss this approximation in section 1.2.3.

To make approximations more accurate, one has to include more information about the density. Such approximations have been very successful and are called Generalized Gradient Approximations (GGA), e.g. PW91 and PBE. The idea to mix in parts of the exact exchange (Hartree Fock) lead to "hybrid" functionals and has become very popular in chemistry; most notably the B3LYP functional [5].

Knowing an expression for the functionals makes it possible to calculate the ground-state density $n_0(\mathbf{r})$ of the interacting particle problem. With the knowledge of $n_0(\mathbf{r})$ we are able to calculate *any* property, given that we knew its functional form.

1.2 Time-dependent density functional theory

The success of ground-state DFT for solving electronic structure problems for static systems gives rise to the question: Is there a time-dependent generalization of the Hohenberg-Kohn theorem and a time-dependent version of the Kohn-Sham-equations ? This time-dependent density functional theory (TDDFT) could then be used to explore time-dependent phenomena, e.g. excited states, polarizibilities, spectra, optical properties and atoms in strong laser fields.

In the time-dependent regime we deal with electronic structure problems which are described by the following Hamiltonian

$$\hat{H}(t) = \hat{T} + \hat{W} + \hat{V}_{ext}(t). \tag{1.20}$$

It is similar to the ground-state Hamiltonian (1.1), except now the external potential operator is time-dependent. The first steps towards a time-dependent DFT came from Bloch [6], introducing the time-dependent Thomas-Fermi method in 1933. Zangwill and Soven [7] and also Peuckert [8] treated rare gas atoms in the linear response regime (see section 1.2.4) within a Kohn-Sham framework. The first formal steps to a rigorous foundation of TDDFT were done by Deb and Ghosh [9, 10, 11, 12], who considered periodic external potentials, and by Bartolotti [13, 14, 15, 16], who explored adiabatic processes. However, modern TDDFT began in 1984, with the Runge-Gross theorem.

1.2.1 The Runge-Gross theorem

The Runge-Gross theorem [17] gave a rigorous foundation to TDDFT. The statement of the Runge-Gross theorem is the existence of a one-to-one mapping between the density $n(\mathbf{r}, t)$ and the time-dependent external potential $v_{ext}(\mathbf{r}, t)$ for a specified initial state $\Psi_0 = \Psi(t_0)$.

Ψ_0 need not to be the ground-state. Sudden switching is included, but adiabatic switching is not, because $v_{ext}(\mathbf{r}, t)$ needs to be Taylor-expandable around t_0.

In their proof Runge and Gross show that two densities $n(\mathbf{r}, t)$ and $n'(\mathbf{r}, t)$ evolving from a common Ψ_0 and under the external potentials $v_{ext}(\mathbf{r}, t)$ and $v'_{ext}(\mathbf{r}, t)$, are always different, if

$$v_{ext}(\mathbf{r},t) \neq v'_{ext}(\mathbf{r},t) + c(t). \tag{1.21}$$

The one-to-one mapping implies, that the wave-function and all expectation values are functionals of the density $n(\mathbf{r},t)$ and the initial-state Ψ_0 :

$$\Psi(t) = \exp\left(-i\alpha(t)\right)\, \tilde{\Psi}[n;\Psi_0](t) \tag{1.22}$$

$$O[n;\Psi_0] = \langle\, \tilde{\Psi}[n;\Psi_0](t)|\hat{O}(t)|\tilde{\Psi}[n;\Psi_0](t)\,\rangle. \tag{1.23}$$

The phase factor in (1.22) appears because the potential $v_{\text{ext}}[n;\Psi_0](\mathbf{r},t)$ can be determined only up to a purely time-dependent function (1.21). However the phase cancels out for the expectation value $\langle\, \hat{O}\,\rangle(t)$ of an operator $\hat{O}$.

So far we know the Runge-Gross theorem, but like in the ground-state problem the knowledge of the one-to-one mapping itself, does not help to solve the problem in practice. So we may ask, if we could also introduce a Kohn-Sham system here.

1.2.2 The time-dependent Kohn Sham equations

The Runge-Gross theorem is also true for the special case that $\hat{W} \equiv 0$. We call this system of non-interacting particles the time-dependent Kohn Sham system

$$i\frac{\partial}{\partial t}\phi_j(\mathbf{r},t) = \left(-\frac{\nabla^2}{2} + v_s[n;\Phi_0](\mathbf{r},t)\right)\phi_j(\mathbf{r},t) \tag{1.24}$$

$$n(\mathbf{r},t) = n_s(\mathbf{r},t) = \sum_{j=1}^{N} |\phi_j(\mathbf{r},t)|^2 \tag{1.25}$$

$$\Phi = \frac{1}{\sqrt{N!}}\,\det\,\{\phi_i(\mathbf{r}_k)\}\,. \tag{1.26}$$

Similar to the ground-state case we apply the following reasoning:

1. We assume that there *exists* a single particle potential $v_s(\mathbf{r},t)$, so that the density $n_s(\mathbf{r},t)$ (1.25) matches the density of the interacting case $n(\mathbf{r},t)$.
   This assumption gives rise to the question of v-representability: It was shown, that for a given (interacting) density $n(\mathbf{r},t)$ a local single particle potential $v_s[n;\Phi_0](\mathbf{r},t)$ always exists under certain restrictions on the initial states [18, 19].

2. The Runge-Gross theorem can be applied and guarantees the uniqueness of $v_s[n;\Phi_0](\mathbf{r},t)$, which is determined by the density and the initial state up to a purely time-dependent function.

   In other words, once we assume the existence of $v_s(\mathbf{r},t)$, we are in principle able to calculate the properties we are interested in, using the Kohn-Sham system.

In the time-dependent case $v_s[n;\Phi_0]$ is given by (compare to (1.19))

$$v_s[n;\Phi_0](\mathbf{r},t) = v_{\mathrm{ext}}[n;\Psi_0](\mathbf{r},t) + \int d\mathbf{r}' \frac{n(\mathbf{r}',t)}{|\mathbf{r}-\mathbf{r}'|} + v_{xc}[n;\Phi_0;\Psi_0](\mathbf{r},t). \tag{1.27}$$

To start a calculation we have to find the Kohn Sham orbitals $\phi_{0,j}(\mathbf{r})$ which reproduce the initial density $n(\mathbf{r},t_0)$ and the divergence of the initial current $\nabla\cdot\mathbf{j}(\mathbf{r},t_0)$ [18] of Ψ_0. But there is in general an infinite number of Slater determinants Φ_0, which satisfy this. In principle the functional v_{xc} will depend on the initial state Ψ_0 of the interacting system and the choice of the initial non interacting state Φ_0: $v_{xc} = v_{xc}[n;\Phi_0;\Psi_0](\mathbf{r},t)$. We can overcome this initial state difficulty [19] by starting in a ground-state at t_0. Then it is possible to apply the Hohenberg-Kohn theorem, so $\Psi_0 = \Psi_0[n_0]$ is a functional of the ground-state density. Thus the functional $v_s[n_0;\Phi_0](\mathbf{r},t) = v_s[n_0](\mathbf{r},t)$ depends only on the density. Fortunately this applies to a large class of problems.
It is important to realize that TDDFT is in principle exact; in contrast to time-dependent Hartree Fock (TDHF) it includes contributions from correlation. However, in practice the accuracy depends on the applied functional for v_{xc}. The big practical advantage of the TDDFT calculations compared to TDHF computations is the locality of the potential $v_s[n;\Phi_0](\mathbf{r},t)$. It is much cheaper to perform TDDFT calculations than TD Hartree Fock or TD Configuration Interaction (CI). Unlike the ground-state case, TDDFT does not involve a self-consistency cycle.
The most common approximation for v_{xc} is a time-dependent version of the Local Density Approximation (LDA), the adiabatic LDA or ALDA.

1.2.3 The adiabatic local density approximation (ALDA)

Since the exact form of $v_{xc}[n;\Phi_0;\Psi_0](\mathbf{r},t)$ is unknown, it is necessary to develop an approximate expression. A popular approximation for $v_{xc}[n](\mathbf{r})$ in ground-state DFT was the Local Density Approximation (LDA), which uses the exchange correlation potential of the homogeneous electron gas $v_{xc}^{hom}[n]$; we shall discuss this ground-state approximation first.

The expression is usually given in terms of the exchange correlation energy per particle ϵ_{xc} of the uniform electron gas:

$$\begin{aligned} v_{xc}^{LDA}(\mathbf{r}) &= \frac{\delta E_{xc}[n]}{\delta n(\mathbf{r})} && (1.28) \\ v_{xc}^{LDA}(\mathbf{r}) &= \frac{d}{dn}(n\,\epsilon_{xc})\bigg|_{n(\mathbf{r})} && (1.29) \end{aligned}$$

$E_{xc}[n]$ can be split into separate exchange and correlation parts and thus also ϵ_{xc} can be split

$$\epsilon_{xc}^{hom} = \epsilon_x^{hom} + \epsilon_c^{hom}. \tag{1.30}$$

The exchange energy of the homogeneous electron gas can be written analytically

$$E_x^{hom} = -\frac{3}{4}\left(\frac{3}{\pi}\right)^{\frac{1}{3}} \int d\mathbf{r}\; n^{\frac{4}{3}}(\mathbf{r}). \tag{1.31}$$

The correlation part ϵ_c^{hom} is found via many-body perturbation theory [20] and with the help of accurate Monte-Carlo integrations. In general, there are different parameterizations for ϵ_c^{hom}. In the high density limit ϵ_c^{hom} the correlation energy per particle is given by

$$\begin{aligned} \epsilon_c^{hom} &= \{0.0622\ln(r_s) - 0.094 + O(r_s\ln(r_s))\}\,\mathrm{Ry} && (1.32) \\ r_s &= \frac{3}{4\pi}\left(\frac{1}{n}\right)^{-\frac{1}{3}} && (1.33) \end{aligned}$$

The variable r_s is called the Wigner-Seitz radius and it may be understood as the radius of the sphere that contains one particle of the system.

An approximation for $v_{xc}[n;\Phi_0;\Psi_0](\mathbf{r},t)$ in TDDFT is to use LDA with a time-dependent density, i.e. $v_{xc} = v_{xc}^{LDA}[n(\mathbf{r},t)]$. This approximation is known as the adiabatic or time-dependent LDA (ALDA or TDLDA). Naively, one expects that it is only accurate for slowly varying systems in space and time: In space, because it is constructed for a homogeneous system, and in time because of the application of static LDA, which is local in time.

Currently ALDA is used in most applications, mainly within linear response.

In linear response theory (see section 1.2.4) it is common to use the exchange correlation (xc) kernel

$$f_{xc}[n_0](\mathbf{r},\mathbf{r}',t-t') = \left.\frac{\delta v_{xc}[n](\mathbf{r},t)}{\delta n(\mathbf{r}',t')}\right|_{n=n_0} \tag{1.34}$$

If we insert (1.29) and take the Fourier transform with respect to $(t-t')$

$$f_{xc}^{ALDA}[n_0](\mathbf{r},\mathbf{r}',t-t') = \delta(t-t')\delta(\mathbf{r}-\mathbf{r}')\frac{d^2}{dn^2}\left.\left(n\epsilon_{xc}^{hom}(n)\right)\right|_{n=n_0(\mathbf{r})} \tag{1.35}$$

$$f_{xc}^{ALDA}[n_0](\mathbf{r},\mathbf{r}';\omega) = \delta(\mathbf{r}-\mathbf{r}')\frac{d^2}{dn^2}\left.\left(n\epsilon_{xc}^{hom}(n)\right)\right|_{n=n_0(\mathbf{r})}. \tag{1.36}$$

we realize that (1.36) is frequency independent. Also, the ALDA exchange correlation potential is independent of Φ_0 and Ψ_0, so it completely neglects the initial state dependence as well as any memory dependence. Attempts to include memory effects can be found in [21], [22] and [23] .

The development of more accurate functionals for TDDFT is yet at a very early stage. The construction is guided by several known constraints [24], i.e. Newton's third law (the net external exchange-correlation force and torque must be zero) and translational invariance, in form of the Harmonic Potential Theorem (see 2.1.2), which is special case of the generalized Kohn theorem [25]. An exact condition addressing memory dependence can be found in [26].

To make the construction of new functionals possible it is necessary to test different aspects of existing functionals and compare them to exact calculations. This is the major motivation of our work in Hooke's atom.

1.2.4 Linear response and applications

Since many problems in the time-dependent regime are treated within linear response theory, a brief derivation of the linear density response function is given in the following. It is possible to derive a formally exact expression for the linear density response $n_1(\mathbf{r},t)$ of an interacting many body system in terms of the response function χ_s of the non-interacting Kohn-Sham system.

We assume the external potential has the form

$$v_{ext}(\mathbf{r},t) = \begin{cases} v_0(\mathbf{r}) & t \leq t_0 \\ v_0(\mathbf{r}) + v_1(\mathbf{r},t) & t > t_0 \end{cases} \tag{1.37}$$

and that the system is at zero temperature and begins in its ground-state Ψ_0. The latter assumption helps to get around the initial state dependence, as mentioned in section (1.2.3).

First we expand $n[v_{ext}](\mathbf{r},t)$ around $n[v_0](\mathbf{r})$ to the first order

$$\begin{aligned} n_1(\mathbf{r},t) &= n[v_{ext}](\mathbf{r},t) - n[v_0](\mathbf{r},t) \qquad (1.38)\\ &= \iint d\mathbf{r}'dt'\ \chi(\mathbf{r},\mathbf{r}',t-t')\, v_1(\mathbf{r}',t') + \ldots \\ \text{where} \qquad \chi[n_0](\mathbf{r},\mathbf{r}',t-t') &= \left.\frac{\delta n[v_{ext}](\mathbf{r},t)}{\delta v_{ext}(\mathbf{r}',t')}\right|_{v_0[n_0]} \qquad (1.39) \end{aligned}$$

Because the Kohn-Sham system has exactly the same density response, we also have

$$\begin{aligned} n_1(\mathbf{r},t) &= \iint d\mathbf{r}'dt'\ \chi_s(\mathbf{r},\mathbf{r}',t-t')\, v_{s,1}(\mathbf{r}',t') \qquad (1.40)\\ \text{with} \qquad \chi_s[n_0](\mathbf{r},\mathbf{r}',t-t') &= \left.\frac{\delta n[v_s](\mathbf{r},t)}{\delta v_s(\mathbf{r}',t')}\right|_{v_s[n_0]}. \qquad (1.41) \end{aligned}$$

Applying the chain rule for functional derivatives to (1.39) the response function becomes

$$\chi[n_0](\mathbf{r},\mathbf{r}',t-t') = \iint d\mathbf{x}d\tau\ \left.\frac{\delta n(\mathbf{r},t)}{\delta v_s(\mathbf{x},\tau)}\frac{\delta v_s(\mathbf{x},\tau)}{\delta v_{ext}(\mathbf{r}',t')}\right|_{n_0}. \tag{1.42}$$

Evaluating the functional derivative $\left.\frac{\delta v_s(\mathbf{r},t)}{\delta v_{ext}(\mathbf{r}',t')}\right|_{n_0}$ using the definition of $v_s[n]$ (1.27), we get a self consistent expression similar to a Dyson equation

$$\begin{aligned} \chi[n_0](\mathbf{r},\mathbf{r}',t-t') &= \chi_s(\mathbf{r},\mathbf{r}',t-t') + \iint d\mathbf{x}d\tau \iint d\mathbf{x}'d\tau'\ \chi_s(\mathbf{r},\mathbf{x},t-\tau) \\ &\times \left(\frac{\delta(\tau-\tau')}{|\mathbf{x}-\mathbf{x}'|} + f_{xc}[n_0](\mathbf{x},\mathbf{x}',\tau-\tau')\right) \chi(\mathbf{x}',\mathbf{r}',\tau'-t') \qquad (1.43) \end{aligned}$$

where $f_{xc}[n_0](\mathbf{r},\mathbf{r}',t-t')$ is the exchange correlation kernel (1.34), which has to be approximated in practice.

The equations (1.38), (1.40) and (1.43) together yield

$$\begin{aligned} v_{s,1}(\mathbf{r}',t') &= v_1(\mathbf{r}',t') + \int d\mathbf{x}\frac{n_1(\mathbf{x},t')}{|\mathbf{x}-\mathbf{r}'|} \\ &\quad + \iint d\mathbf{x}'d\tau'\ f_{xc}[n_0](\mathbf{r}',\mathbf{x},t'-\tau)n_1(\mathbf{x},\tau) \end{aligned} \tag{1.44}$$

Equation (1.40) together with (1.44) then gives an expression for the linear density response.

Most of the applications of TDDFT involve the calculation of excitation energies from TDDFT [27]. These lie at the poles of the response function χ (1.43) in the frequency domain.

The Fourier transform of χ_s has the analytical expression

$$\chi_s(\mathbf{r},\mathbf{r}',\omega) = \sum_{j,k} (o_k - o_j)\frac{\phi_j(\mathbf{r})\phi_k^*(\mathbf{r})\phi_j^*(\mathbf{r}')\phi_k(\mathbf{r}')}{\omega - (\epsilon_j - \epsilon_k) + i\eta}, \tag{1.45}$$

where o_j, o_k are the occupation numbers of the Kohn-Sham orbitals. The summation runs over all occupied and unoccupied states, including continuum states.

A way to extract excitation energies or oscillator strengths [28] from the interacting system is to solve the integral equation for χ (1.43) directly with an approximation for f_{xc} and (1.45). The possibility to calculate excitation energies has been implemented in Gaussian98, a standard tool in computational chemistry.

We have derived the expression for the first order density response in terms of the non-interacting response function χ_s (1.40). With the knowledge of $n_1(\mathbf{r},\omega)$, we can also calculate the dynamic polarizability for a finite system within the dipole approximation

$$\alpha(\omega) = -\frac{2}{E}\int d\mathbf{r}\ z\, n_1(\mathbf{r},\omega) \tag{1.46}$$

where $n_1(\mathbf{r},\omega)$ is the Fourier transform of the linear density response (1.40)

$$\begin{aligned} n_1(\mathbf{r},\omega) &= \int d\mathbf{y}\ \chi_s(\mathbf{r},\mathbf{y};\omega)\, v_1(\mathbf{y},\omega) \\ &\quad + \iint d\mathbf{y}d\mathbf{y}'\ \chi_s(\mathbf{r},\mathbf{y};\omega)\left(\frac{1}{|\mathbf{y}-\mathbf{y}'|} + f_{xc}[n_0](\mathbf{y},\mathbf{y}';\omega)\right) n_1(\mathbf{y}',\omega). \end{aligned} \tag{1.47}$$

The photoabsorption cross-section is calculated from the dynamic polarizability

$$\sigma(\omega) = \frac{4\pi\omega}{c}\Im\alpha(\omega), \tag{1.48}$$

Here we mention just a few examples, where the theory has been applied to different kind of systems.

A time-dependent density functional calculation on the electronic absorption spectrum of free base porphin [29] was done by Gisbergen et al. The application of TDDFT yields new calculation schemes [30]. Heinze et al. [31] present an efficient way to calculate molecular excitation energies and apply their scheme to benzene, naphthalene and the higher linearly annelated polycyclic aromatic hydrocarbons anthracene to heptacene. The calculation of the visible spectrum of chlorophyll α [32] shows that even systems of biological interest can be examined.

Applications to excited states in solids yield poor results. The problem is due to the xc-kernels which are optimized for atoms, and have an incorrect long wavelength limit [33].

Gisbergen et al. [34] studied the frequency dependent polarizibility and van der Waals dispersion coefficients for polyatomic molecules and included ALDA in the Amsterdam DFT software package [35]. They found results comparable to time-dependent Hartree-Fock and Many-body-perturbation-theory calculations, which are computationally more expensive. They also studied molecules containing transition metals ($Mn0_4^-$, $Ni(CO)_4$, $Mn_2(CO)_{10}$) [36] with results comparable in accuracy to most elaborate ab initio calculations.

The optical response of clusters has been studied: Lerme et al. [37] investigated the optical response of free and matrix-embedded gold metal clusters within ALDA and Yabana and Bertsch [38] looked at small silver clusters. Yabana and Bertsch also calculated the optical activity of methyloxirane and C_{76} [39].

The photoabsorption spectra of small semiconductor and metal clusters was examined within TDDFT by Rubio et al. [40]. A good agreement with experimental results was found for the absorption spectra and optical gaps in nanocrystalline Silicon (up to 250 atoms) [41].

An application of TDDFT within ALDA, that has become very popular recently are atoms in strong laser-fields [42], i.e. Bauer and Ceccherini [43] study the interaction of Ne with short and intensive laser-pulses. They find a good agreement with the Ne^+ yield but they also state that the observation of the NSI-"knee" was not satisfactory compared with experiment. In [44] the double ionization of He in strong fields was studied. Another example is the study of Laser excitation in Na clusters by Reinhard et al. [45].

All these applications employ ALDA. In the linear response regime, good results are found in comparison with experimental data or computationally more expensive methods. But there is no calculation in the literature, where ALDA is compared to a time-dependent system that can be solved exactly.

Chapter 2

Experiment (computational)

2.1 The model system: Hooke's atom

The goal of this work is to test ALDA on an exactly soluble system. The test should provide further insight in the performance of ALDA. We saw in the previous section, that ALDA is successfully used in many applications. But at this time the understanding of when and how ALDA yields these good results is far behind these numerous applications. A deeper understanding might also be helpful in the construction of new functional approximations for time-dependent density functional theory.

2.1.1 Time independent properties

In physics simple models often play an important role. One model system that has become more and more exploited [46, 47] within DFT is called Hooke's atom. It consists of two interacting electrons in a harmonic potential $v_{ext} = \frac{1}{2}k\,r^2$. The Hamiltonian is given by

$$\hat{H} = -\frac{1}{2}\nabla^2_{r_1} - \frac{1}{2}\nabla^2_{r_2} + \frac{1}{2}k\left(r_1^2 + r_2^2\right) + \frac{1}{|\mathbf{r}_2 - \mathbf{r}_1|} \tag{2.1}$$

One might argue that this system is rather unphysical and not a good model for an atom because it is not possible to ionize it. On the other hand harmonic potentials are used in the description of quantum dots as confining potentials [48] for the electrons. Hooke's atom has become an important model, because it is analytically solvable for a denumerably infinite set of force constants k [49] and for all other force constants the numerical solution is easy.

With the introduction of center of mass and relative coordinates,

$$\mathbf{R} = \frac{1}{2}\mathbf{r}_1 + \frac{1}{2}\mathbf{r}_2 \tag{2.2}$$

$$\mathbf{u} = \mathbf{r}_2 - \mathbf{r}_1 \tag{2.3}$$

it is possible to separate the Hamiltonian (2.1) into

$$\hat{H} = \hat{H}_R + \hat{H}_u \tag{2.4}$$

$$\hat{H}_R = -\frac{1}{2m_R}\nabla_R^2 + \frac{1}{2}m_R\Omega^2 R^2 \tag{2.5}$$

$$\hat{H}_u = -\frac{1}{2m_u}\nabla_u^2 + \frac{1}{2}m_u\Omega^2 u^2 + \frac{1}{u} \tag{2.6}$$

$$m_R = 2 \qquad m_u = \frac{1}{2}. \tag{2.7}$$

The Schrödinger equation separates into two equations: one for the center of mass coordinate $\mathbf{R}$, which describes the 3d harmonic oscillator and the other for the relative coordinate $\mathbf{u}$. The $\mathbf{u}$ equation is similar to the harmonic oscillator but has an additional Coulomb potential $\frac{1}{|\mathbf{u}|}$.

The first work towards an analytical solution of Hooke's atom was done in [50] for certain values for the force constant k. The ground-state density for a force constant $k = \frac{1}{4}$ is

$$\begin{aligned} n(r) &= \frac{\sqrt{2}}{4\pi(5\sqrt{2}+8)r}\exp\left[-\frac{r^2}{2}\right] \\ &\times\left(7r + r^3 + \frac{8r}{\sqrt{2\pi}}\exp\left[-\frac{r^2}{2}\right] + 4(1+r^2)\ \mathrm{erf}\left[\frac{r}{\sqrt{2}}\right]\right) \end{aligned} \tag{2.8}$$

With the knowledge of the exact ground-state density, it is possible to construct the exact form of the Kohn-Sham potential $v_s(r)$ by inverting the Kohn-Sham equation (1.9) and inserting the known density (2.8). From the definition of v_s (1.19) the exchange correlation potential v_{xc} can be evaluated. The exact values can be compared with functional approximations [51].

The analytical solution of Hooke's atom (for certain k values) allows also the exact calculation of properties [52], e.g. pair-correlation density, the Fermi and Coulomb holes, kinetic-energy-density tensors.

For general values of k one can easily solve the equation for the relative coordinate numerically, because the equations still separate.

2.1.2 Time dependent properties

Hooke's atom is also an important model in the time-dependent domain, where one introduces a time-dependent perturbation. The choice in our work was to replace the

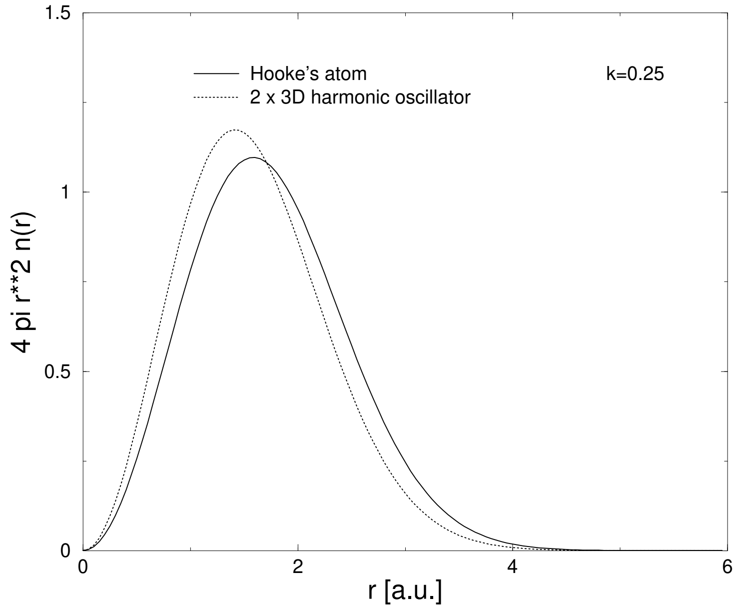

Figure 2.1: Density of Hooke's atom and density of two non-interacting 3d harmonic oscillators.

force constant k with a time-dependent one

$$k(t) = \bar{k} - \epsilon \cos(\omega t). \tag{2.9}$$

The values of the force constant oscillates around the average value $\bar{k}$. The one electron version is a Mathieu oscillator, whose classical dynamics have been studied in detail; in particular the regions of stability and instability [53].

One might argue that a more useful approach would be to add an external field in dipole approximation $\hat{H}_1 = -\mathbf{F} \cdot (\mathbf{r_1} + \mathbf{r_2}) \cos \omega t$. But this kind of perturbation just couples to the center of mass system (2.5) via (2.2). This has certain consequences, e.g. $V_{ee}(t) = V_{ee}(0)$ and therefore $E_{xc}(t) = E_{xc}(0)$ and $E_c(t) = E_c(0)$, because the interaction only depends on the relative coordinate. This potential also fulfills the assumptions of the Harmonic Potential Theorem (HPT) [54]. The HPT is applicable for interacting many-electron systems in an external harmonic potential plus an external force field $-\mathbf{G}(t) \cdot \mathbf{r}$. The statement is that the time-dependent density is rigidly related to the ground-state density by

$$n(\mathbf{r}, t) = n_0(\mathbf{r} - \mathbf{X}(t)), \tag{2.10}$$

where $\mathbf{X}(t)$ is the position of the origin of the moving frame with respect to rest frame. So with this kind of perturbation only a small set of possible time-dependent behaviour can be observed.

With a time-dependent force constant $k(t) = \bar{k} - \epsilon \cos \omega t$ one can cover a more general time-dependent behaviour of the system and it is still possible to separate the problem in center of mass and relative coordinates. The Hooke's atom with this $k(t)$ is explored in [55] and [56]. The second article focuses on time-dependent energy components and compares them to ground-state values. The results are the motivation for this work.

If we start the time-dependent Hooke's atom in the ground-state, a spin-singlet, it will always remain spherically symmetric and in the spin singlet. This makes it possible to solve the time-dependent Schrödinger equation numerically exactly in a simple way (see section 2.1.3) and no approximation is needed. From the exact wave-functions, we can calculate the density $n(\mathbf{r}, t) = n(r, t)$.

The knowledge of the exact density gives us the possibility to calculate the correlation energy $E_c(t)$ for the system. To achieve this, we have to do the following steps. First we invert the Kohn-Sham equation. Since the two electrons are in a spin singlet, we may write the doubly occupied spatial orbital as

$$\phi(\mathbf{r}, t) = A(\mathbf{r}, t) \exp(\imath \alpha(\mathbf{r}, t)) \tag{2.11}$$

$$n(\mathbf{r}, t) = 2 \left| \phi(\mathbf{r}, t) \right|^2 \tag{2.12}$$

Next we invert the time-dependent Kohn-Sham equation (1.24)

$$\left\{ -\frac{1}{r^2} \frac{\partial}{\partial r} r^2 \frac{\partial}{\partial r} + v_s(r, t) \right\} \phi(r, t) = \imath \frac{\partial}{\partial t} \phi(r, t) \tag{2.13}$$

to obtain the potential v_s for the ground-state ($l = 0$). This gives two relations, because v_s has to be real. The calculation yields

$$v_s = \frac{1}{2r} \frac{n'}{n} + \frac{1}{4} \frac{n''}{n} - \frac{1}{8} \left(\frac{n'}{n} \right)^2 - \frac{1}{2} \alpha'^2 \frac{\partial \alpha}{\partial t} \tag{2.14}$$

$$\alpha' = \frac{1}{n\, r^2} \int_0^r dr' \; \dot{n}(r', t)\, r'^2 \tag{2.15}$$

With the knowledge of v_s we are now able to construct v_{xc} using (1.27)

$$v_{xc}(r, t) = v_s(r, t) - v_{ext} - \int d\mathbf{r}' \; \frac{n(r', t)}{|\mathbf{r} - \mathbf{r}'|} \tag{2.16}$$

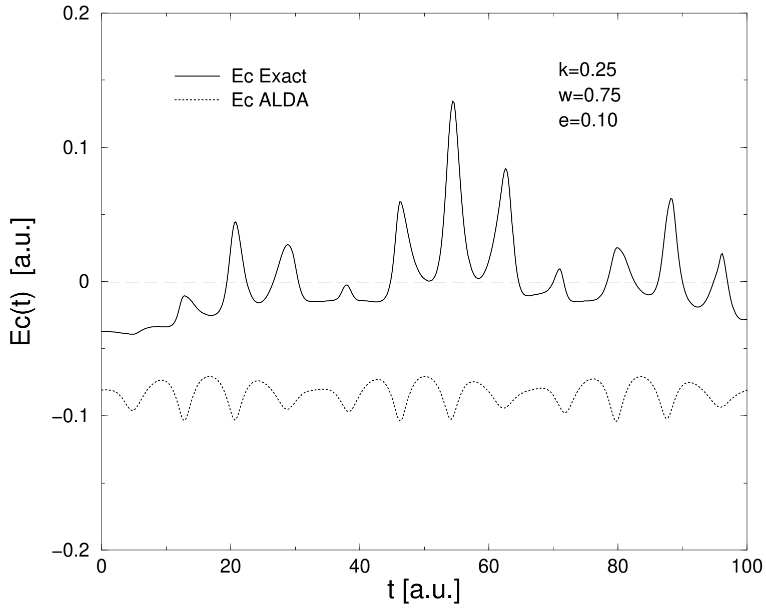

Figure 2.2: $E_c(t)$ for Hooke's atom with $\bar{k} = 0.25, \omega = 0.75, \epsilon = 0.1$. The solid line is the exact calculation, while the dotted stands for the ALDA calculation.

From [55] we know that

$$E_{xc}(t) = E_{xc}(0) + \int_0^t dt' \int d\mathbf{r}\, v_{xc}(\mathbf{r}, t')\, \dot{n}(\mathbf{r}, t'). \tag{2.17}$$

Since we are dealing with a two electron system the exchange energy is

$$E_x(t) = -\frac{1}{2} E_H(t) \tag{2.18}$$

$$E_H(t) = \frac{1}{2} \iint d\mathbf{r} d\mathbf{r}' \; \frac{n(\mathbf{r}, t)\, n(\mathbf{r}', t)}{|\mathbf{r} - \mathbf{r}'|} \tag{2.19}$$

So, having the exact density we can simply evaluate v_s, $E_H(t)$, v_{xc}, E_{xc} and extract

$$E_c(t) = E_{xc}(t) - \frac{1}{2} E_H(t) \tag{2.20}$$

The figure 2.2 shows the correlation energy for a run with $\bar{k} = 0.25, \omega = 0.75, \epsilon = 0.1$. We notice that the correlation energy becomes positive after a certain time. In ground-state DFT the correlation is always negative $E_c[n] \leq 0$, due to the variational principle. In any adiabatic approximation then $E_c[n]$ cannot become positive.

In fact the correlation energy for the same parameters evaluated with ALDA looks quite different from the exact calculation (see figure 2.2). Since ALDA uses LDA with the

time-dependent density, the correlation energy evaluated with the ALDA functional stays always negative. In other words ALDA is not able to cover this effect. We might ask for general properties: How accurate is ALDA ? In particular, does ALDA still reproduce the right density, even if not E_c ?
An answer for Hooke's atom to this question will be given in section 2.2.

2.1.3 Numerical considerations

For the comparison of the exact solution with the ALDA basically two programs are used. The first one calculates the solution of the time-dependent Schrödinger equation and evaluates the *exact* Kohn-Sham values, i.e. $E_c(t), T_s(t), \langle r^2 \rangle(t)$. The second one solves the time evolution using the ALDA.
We refer to the first program as the exact calculation and to the second one as ALDA calculation.
To solve the time-dependent Schrödinger equation we employ the Crank-Nicolson method [57], which is to second order accurate in space and time [58]. The Crank-Nicolson method uses the fact that the time-evolution operator has to be unitary. This yields great stability. In the following we want to give the basic scheme of the Crank-Nicolson method. The time-evolution operator is given by

$$\hat{U}(t,0) = \hat{\mathrm{T}}\exp\left\{-i\int_0^t dt' H(t')\right\} \tag{2.21}$$

$$\hat{U}(t,0)|\Psi(0)\rangle = |\Psi(t)\rangle \tag{2.22}$$

The infinitesimal expression of this operator is

$$\hat{U}(t+dt,t)|\Psi(t)\rangle = \left(1 - i\hat{H}dt\right)|\Psi(t)\rangle \tag{2.23}$$

$$= \hat{U}(t+dt,t+\frac{dt}{2})\hat{U}(t+\frac{dt}{2},t)|\Psi(t)\rangle \tag{2.24}$$

where we split the infinitesimal time-evolution operator in two parts. Now we rewrite the above expression by multiplying the inverse of the operator

$$\hat{U}(t+\frac{dt}{2},t)|\Psi(t)\rangle = \hat{U}^{-1}(t+\frac{dt}{2},t)|\Psi(t+dt)\rangle \tag{2.25}$$

$$\left(1-\frac{i}{2}\hat{H}dt\right)|\Psi(t)\rangle = \left(1+\frac{i}{2}\hat{H}dt\right)|\Psi(t+dt)\rangle \tag{2.26}$$

The last equation (2.26) provides the basic scheme for the Crank-Nicolson method. To apply it, we have to discretize $\hat{H}(t)$. For the discretization we employ a variable transformation for the position $r \epsilon \{0, \infty\}$ to a uniform grid $y \epsilon \{1, 0\}$

$$y = \frac{1}{1 + \frac{r}{r_0}} \tag{2.27}$$

$$r = r_0 \left(\frac{1}{y} - 1 \right) \tag{2.28}$$

So the important region of the wave-function is sampled with more grid points ($r \to 0$) and the grid gets sparse for ($r \to \infty$). The discretization and the coordinate transform yield the alogrithm for the time-evolution.

We start both calculations in their ground-state. The ground-state of the exact calculation is given by the ground-state of the 3d harmonic oscillator in the center of mass system and the ground-state of the relative coordinate system (2.6). To get the latter one we employ a matrix method. We calculate the Hamiltonian matrix for a gaussian basis set and then find the eigenvectors, so we get the ground-state for arbitrary values of k.

We use an imaginary time propagation (ITP) method to make the ground-state consistent with the numerical grid. In the limit of infinite grid-points the "numerical" ground-state will be identical with the true ground-state (see appendix B). The ground-state obtained by the exact formula for the 3d harmonic oscillator and the matrix method is from the point of view of the numerical grid only an approximation. One can think of this procedure as purifying the "numerical" ground-state from higher eigenfunctions.

To check the calculations we monitor the norm during the run, which is supposed to stay fixed, if the size of the time step is small enough. We also check the virial theorem [55] for the exact calculation

$$E_{xc}[n](t) + T_c[n](t) = -\int d\mathbf{r}\, n(\mathbf{r}, t)\, \mathbf{r} \cdot \nabla \cdot v_{xc}[n](\mathbf{r}, t). \tag{2.29}$$

We calculate both sides of the equation (2.29) and compare them.

In the ALDA calculation the Perdew Wang parameterization [59] is used for the LDA. To find the LDA ground-state we have to solve the Kohn-Sham equation self-consistently. Here, we again employ the ITP method, updating the density in each (imaginary) time step and calculating $v_s[n](r)$. As initial guess the wave-function from the exact calculation is used.

2.2 Results

We run the programs for different parameter sets. Before we start analyzing the results, we want to clarify and introduce a few terms. An overview of the certain runs that we will consider are given in table 2.1. It lists the parameter sets, which consist of the values for $\bar{k}$, ω, ϵ and the duration of the perturbation, given in multiples of half periods $\frac{T}{2} = \frac{\pi}{\omega}$. It is convenient to introduce names for the parameter sets. All values are given in atomic units and by frequency we mean the angular frequency $\omega = 2\pi f$.

In the analysis we look at the expectation value $\langle\, r^2(t)\,\rangle$, which has the interpretation

$\bar{k}$	ω	ϵ	duration of the perturbation	name
0.25	0.75	0.10	entire run	generic run
0.25	0.75	0.01	entire run	weak generic
0.25	0.75	0.10	1	generic turned-off

Table 2.1: Overview of run parameters.

of the spread of the density (e.g. for the unperturbed 3d harmonic oscillator with $\bar{k} = 0.25$ the spread of the density $\langle\, r^2\,\rangle = 3.00$). One major question we wish to explore is how does the time-evolving ALDA density compare with the exact one. The time-dependence of the spread reflects very well the time-dependent behaviour of the density, since

$$\langle\, r^2\,\rangle(t) = \frac{4\pi \int dr\ r^4\, n(r,t)}{\underbrace{N}_{=2}} \tag{2.30}$$

To aid our analysis we consider switching off the interaction in Hooke's atom. We are left with two perturbed 3d harmonic oscillators. Since we have two electrons we simply need to double the density of 3d harmonic oscillator to get the non-interacting system. The 3d harmonic oscillator is also straightforward to treat in first order time-dependent perturbation theory. The first order expression for $\langle\, r^2\,\rangle(t)$ in the non-resonant case is given by

$$\langle\, r^2\,\rangle(t) \quad = \quad \frac{3}{2\sqrt{\bar{k}}} + \frac{3\,\epsilon}{\sqrt{\bar{k}}\,(4\bar{k}-\omega^2)}\cos\omega t - \frac{3\,\epsilon\,\omega^2}{4\bar{k}^{3/2}\,(4\bar{k}-\omega^2)}\cos\left(2\sqrt{\bar{k}}t\right) \tag{2.31}$$

So we know, what frequencies we may expect to see in linear response, of course these will be modified slightly in the interacting case. We can then use the expression to distinguish between first or higher order contributions in the following analysis. The derivation of (2.31) is given in appendix A.

Notice, that for $\omega = 2\sqrt{\bar{k}}$ the system is in resonance and we obtain a different expression for $\langle r^2 \rangle(t)$, which contains a factor proportional to t. We do not consider the resonant case here, because an accurate calculation of $\langle r^2 \rangle(t)$ beyond short times is very difficult. The relevant time scale is given by the period of the perturbation frequency, e.g. for $\omega = 0.75$ $T = \frac{2\pi}{\omega} \approx 8$. So by short times we mean a few multiples of the period.

2.2.1 The generic run

We want to look at the generic run, it is parametrized by $\bar{k} = 0.25$, $\omega = 0.75$, $\epsilon = 0.10$. It is "generic" in parameter space, because it neither fulfills the resonance condition, i.e. $\omega = 2\sqrt{\bar{k}}$ nor is it adiabatic. Also, ϵ has an intermediate value, which is beyond the linear response regime.

Figure 2.3 shows the behaviour of $\langle r^2 \rangle(t)$ for the generic run. The figure shows how the density squeezes and spreads out, responding to the oscillating force-constant $k(t)$. First notice the non-interacting 3d harmonic oscillator. We can see that the first order expression (2.31) still resembles most of the features of the perturbed harmonic oscillator. However higher order features are present, because $\epsilon = 0.10$ is not small compared with $\bar{k} = 0.25$. Compared to the interacting system, the 3d harmonic oscillator seems to resemble the trends in the dynamics quite well, but there are differences due to the electron-electron interaction. For example, the density is more spread in the interacting system, so we expect the interacting curve to lie above the non-interacting one.

For the interacting system, the exact and the ALDA calculation seem to match quite well for short times. The largest difference in figure 2.3 seems to be around $t \approx 32$. Note, that the difference at $t = 0$ is due to fact, that we start in the LDA ground-state, whose density is slightly different from the exact ground-state density.

In figure 2.4 we show $\langle r^2(t) \rangle$ for later times. We suppress the first order perturbation theory curve for readability. We notice that there is a beating on top of all three

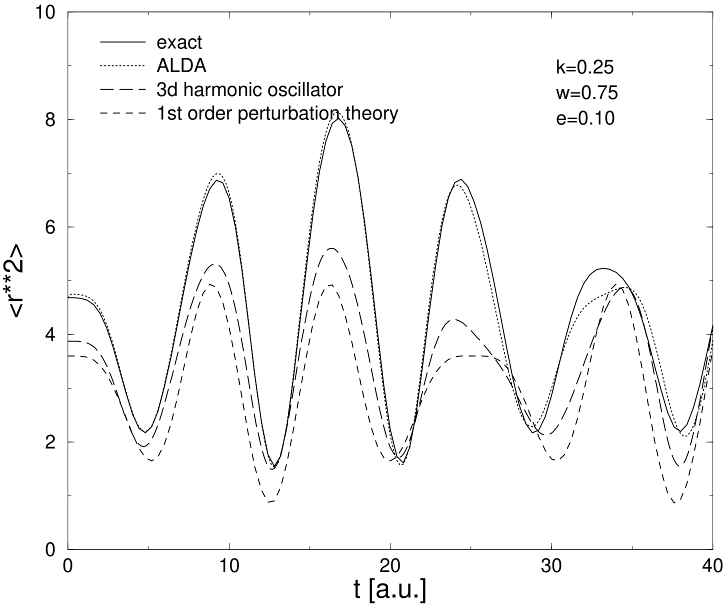

Figure 2.3: The plot shows the time-dependent behaviour of the spread of the density $\langle r^2(t) \rangle$ in the generic run for the Hooke's atom, i.e. the exact run (solid) and the ALDA calculation (dotted), the non-interacting case (3d harmonic oscillator, long-dashed) and $\langle r^2(t) \rangle$ in first order perturbation theory (dashed) for the harmonic oscillator. For this short time range, the ALDA curve lies on top of the exact calculation.

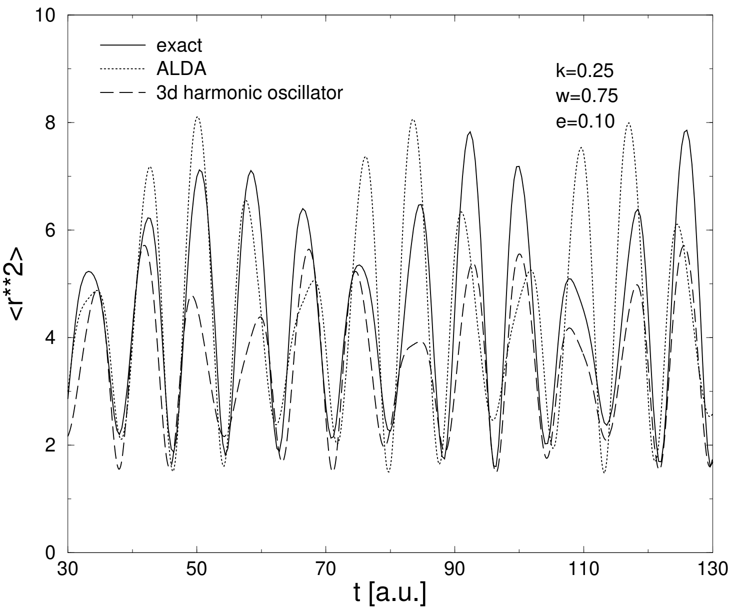

Figure 2.4: For $t \geq 30$ the exact (solid) and the ALDA (dotted) curve differ clearly. We suppress the linear response curve for readability.

oscillating curves. But the period of this beating seems to be different in each case, so that ALDA and the exact calculations have quite different values for $\langle r^2 \rangle(t)$ at larger times.

The densities at $t = 100$ are shown in Figure 2.5. The exact density is far more diffuse

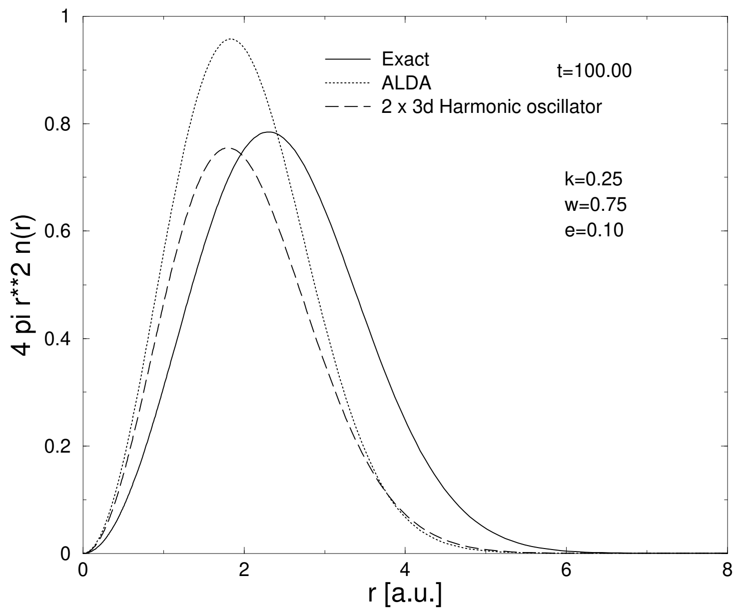

Figure 2.5: This graph illustrates the difference between the ALDA density and the exact density at $t = 100$. The exact density is more spread than the ALDA density.

than the ALDA, which is more concentrated around the origin. Figure 2.5 also shows twice the density of the 3d harmonic oscillator, which happens to be close to the ALDA curve at this time (see also figure 2.4 at t=100).

Before looking more closely at $\langle r^2 \rangle(t)$, we might glance at other quantities. In the previous chapter we have already seen $E_c(t)$ for both calculations. These are quite different even at shorter times. On the other hand in figure 2.6, the exact Kohn-Sham kinetic energy $T_s^{Exact}(t)$ and the approximated $T_s^{ALDA}(t)$ are again matching quite well for $t \leq 30$ but become very different for later times. We observe that the kinetic energy curves and $E_c^{ALDA}(t)$ (given in figure 2.2) resemble the behaviour of the corresponding $\langle r^2 \rangle(t)$, shown in the figures 2.4 and 2.3.

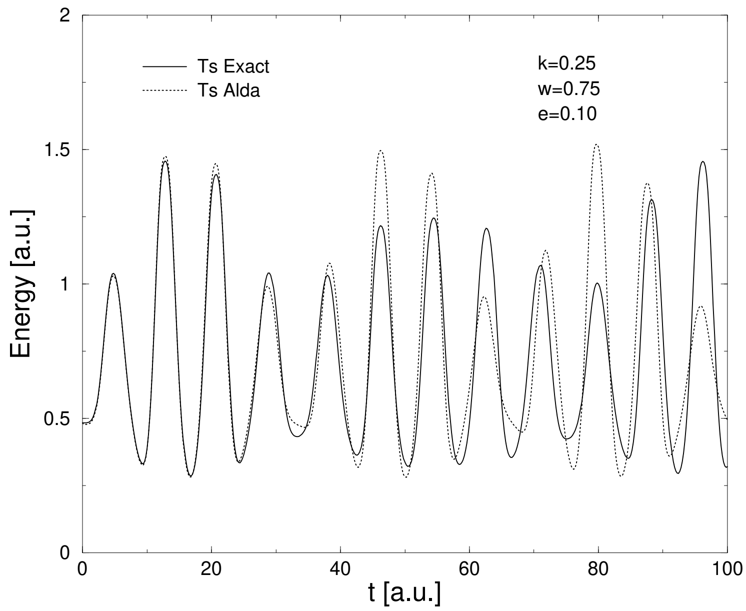

Figure 2.6: $T_s(t)$ for the ALDA and the exact calculation. We see a good matching for short times, but a qualitative difference for larger times.

Fourier analysis

An enlightening way to analyze the time-dependent behaviour of $\langle r^2 \rangle(t)$ is to Fourier transform this quantity. In the following we will look at the peak positions of four different calculations: the exact (solid), the ALDA (dotted), the 3d harmonic (long-dashed) oscillator and the 3d harmonic oscillator in linear response (dashed). Figure 2.7 gives an overview over the frequency range, where we can see the relevant frequency contributions. We will focus on its details in the following.

We use the linear response expression (2.31) to see the influence of the finite duration of the run. The finite duration (a square window in the time domain) causes a $\frac{1}{\omega}$ decay of the peaks in frequency space, which in the limit of infinite duration would change to a δ peak. Comparing the peak width for the other runs with that of the linear response, we can see if the broadness of the peak is simply an effect of the finite duration of the run, or otherwise.

In the overview graph (figure 2.7) we observe several groups of peaks at different frequencies. First we shall focus on the features of the three largest contributions around

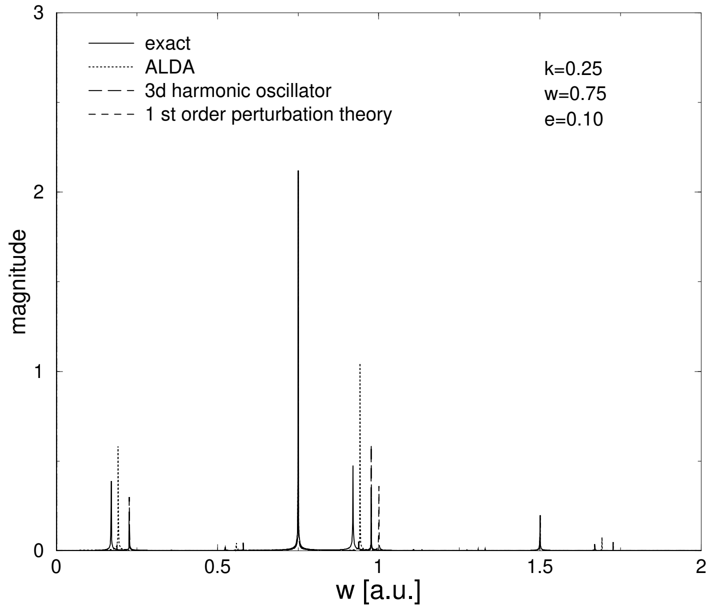

Figure 2.7: This shows the spectrum of $\langle r^2 \rangle(\omega)$ for the generic run. Beyond $\omega = 2.00$ no relevant peaks occur. The graph is meant as an overview, we will focus on the details in the next figures.

$\omega = 0.75,\ 0.95,\ 0.20$. After finding similarities and differences we try to explain these.

We start by looking at the highest group of peaks in figure 2.8 at $\omega = 0.75$. This peak is simple to explain: $\omega = 0.75$ is exactly the frequency of our perturbation . We recall that our perturbation squeezes and releases the harmonic potential with this frequency, so there must be a big contribution to $\langle r^2 \rangle(t)$ for this driving frequency. In figure 2.8 all four curves have their peak value at $\omega = 0.750$.

The next group of peaks in Figure 2.9 is located around $\omega = 0.95$. There we find five peaks: The peak of the linear response formula (2.31) is exactly at $\omega = 1.000$. The 3d harmonic oscillator and the exact calculation have a peak at $\omega = 0.977$. The ALDA calculation shows a contribution at $\omega = 0.942$. The other two peaks belong to the exact calculation, i.e. a very small one at $\omega = 0.938$ and the highest one in this range at $\omega = 0.920$.

The third highest set of peaks is located around $\omega = 0.20$. Here we find the ALDA peak at $\omega = 0.192$, the harmonic peak on top of the exact one at $\omega = 0.227$ and the other exact peaks are at $\omega = 0.170$ and $\omega = 0.188$. Notice that there is no linear

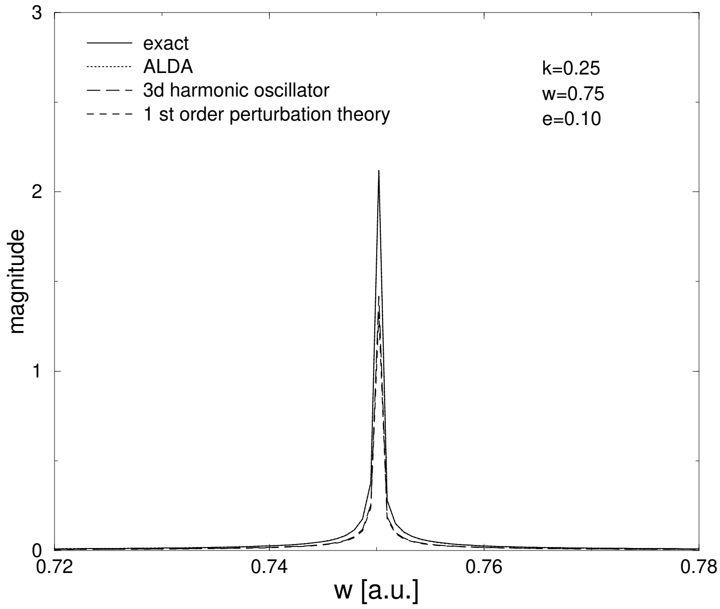

Figure 2.8: This plot shows the spectrum of $\langle r^2 \rangle(\omega)$ for the generic run around $\omega = 0.75$, the perturbation frequency.

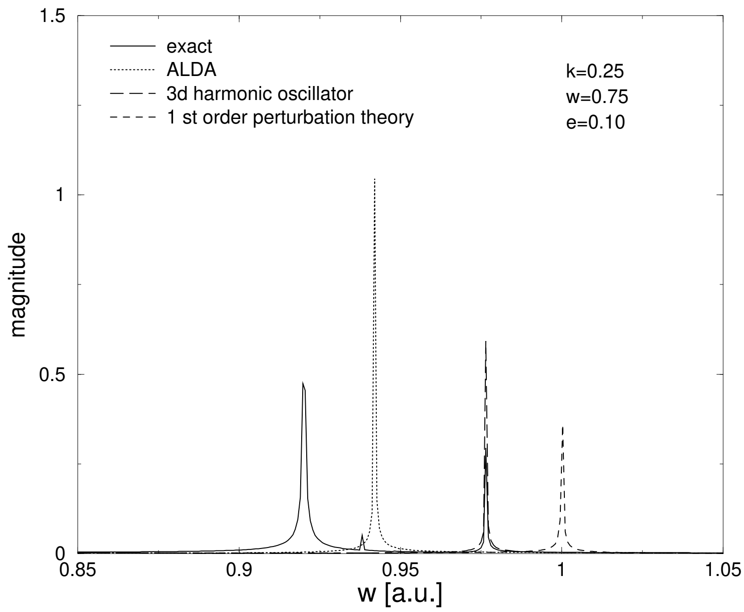

Figure 2.9: The graph shows the spectrum of $\langle r^2 \rangle(\omega)$ for the generic run from $0.85 \leq \omega \leq 1.05$.

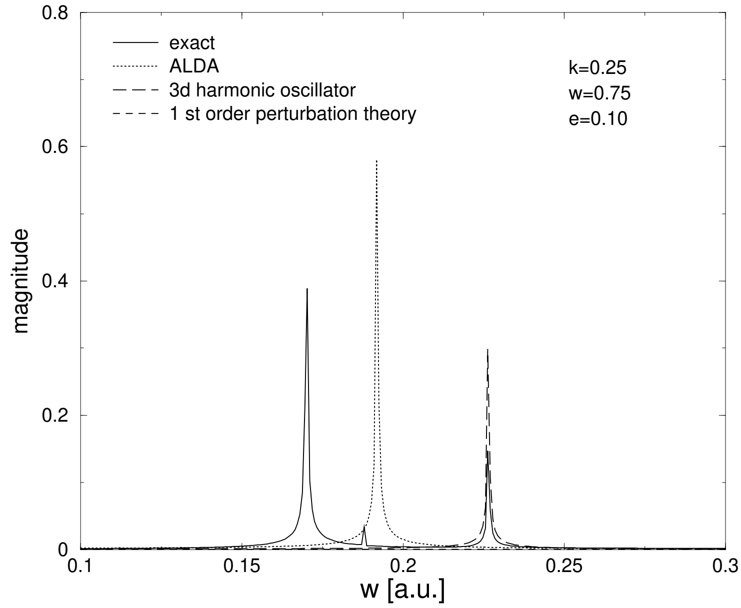

Figure 2.10: We plot the spectrum of $\langle r^2 \rangle(\omega)$ for the generic run from $0.1 \leq \omega \leq 0.3$.

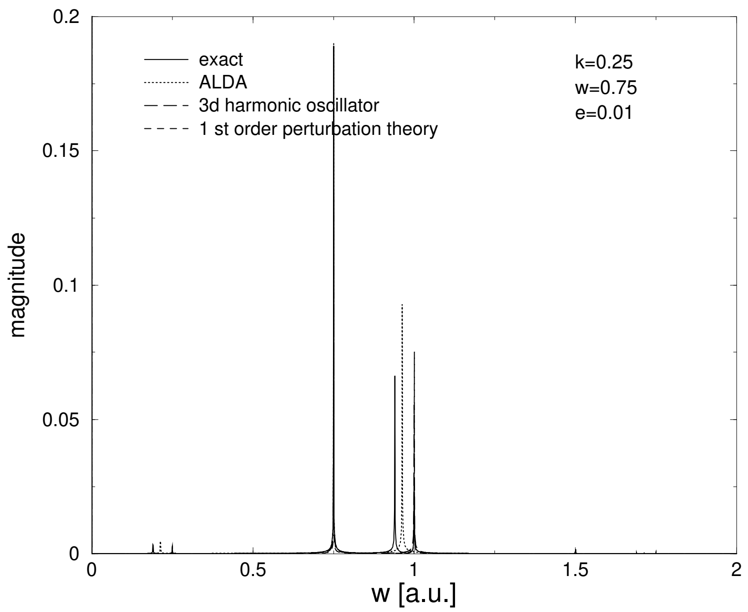

Figure 2.11: This shows the spectrum of $\langle r^2 \rangle(\omega)$ for the weak generic run, where $\epsilon = 0.01$.

response peak. So the 3d harmonic oscillator contribution and the other peaks can not be explained within linear response. This is expected since our perturbation is beyond the linear response regime. Table 2.2 gives an overview of the positions of the peaks for generic run. In this table we also list the results for the weak generic run, which is in the linear response regime.

The reason for the appearance of the multiple exact peaks compared to 3d harmonic

$k = 0.25\, \omega = 0.75$	1st order	3d harmonic oscillator	ALDA	exact		
$\epsilon = 0.1$	0.750	0.750	0.750	0.750	-	-
	1.000	0.977	0.942	0.920	0.977	0.938
	-	0.227	0.192	0.170	0.227	0.188
$\epsilon = 0.01$	0.750	0.750	0.750	0.750	-	-
	1.000	1.000	0.963	0.940	1.000	-
	-	0.250	0.213	0.190	0.250	-

Table 2.2: The table lists frequencies that we find in the spectrum of the generic ($\epsilon = 0.1$) and the weak generic run ($\epsilon = 0.01$). The first three rows show the peak positions for the generic run. Each corresponds to a group of peaks. The last three columns show the exact peaks in the order of their height. The following rows correspond to the weak generic run, which is within the linear response regime. Note that in the last two rows we cannot find a third exact peak, because of the small perturbation.

oscillator is the interaction. Before we explain this in detail and understand the peak positions better, we consider a run, where we turn off the perturbation after one half period. This run is easier to analyze and once we understand the features in this case, we can try to transfer the knowledge to the generic run.

Turning off the perturbation

The behaviour of $\langle r^2 \rangle(t)$ for the turned-off calculation is shown in figure 2.12. In this graph, we see that the ALDA curve is simply oscillating with one frequency and the exact curve has a beating. How can we explain this different behaviour ?

After turning off the perturbation at t_f, so that $k(t) = k(t_f)$ for $t \geq t_f$, we can expand the wave-function in eigenfunctions of the time-independent Hamiltonian with the force

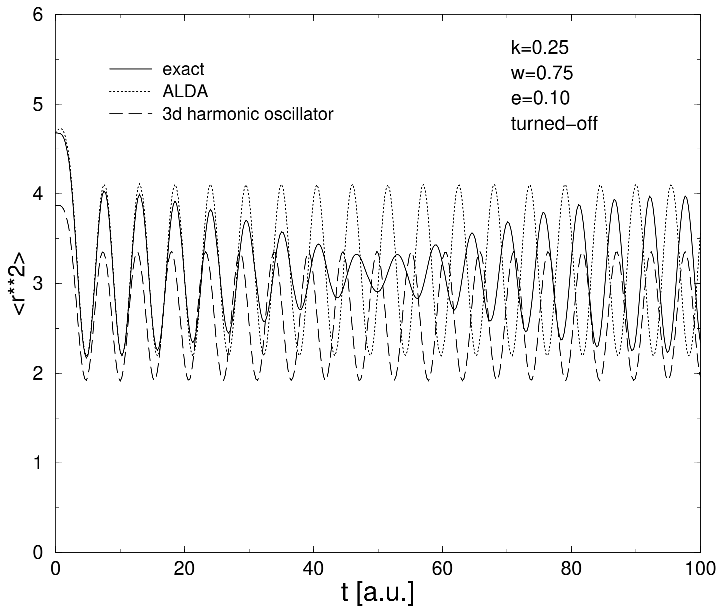

Figure 2.12: This graph shows $\langle r^2 \rangle(t)$ for the generic turned-off run, where the force constant was kept constant after a half period. In contrast to the ALDA curve, the exact calculation shows a beating.

constant $k = k(t_f)$. Because of this time-independence the time evolution is simple for $t \geq t_f$

$$|\Psi(t_f)\rangle = \sum_{n=0}^{\infty} \underbrace{\langle n|\Psi(t_f)\rangle}_{b_n} |n\rangle \tag{2.32}$$

$$|\Psi(t)\rangle = e^{-iH(t-t_f)}|\Psi(t_f)\rangle \tag{2.33}$$

$$= \sum_{n=0}^{\infty} e^{-iE_n(t-t_f)} b_n |n\rangle \tag{2.34}$$

When we calculate the density for this wave-function we get time-dependent cross terms, whose frequency dependence is the difference of the eigenvalues of the Hamiltonian $\hat{H}(t_f)$, i.e. the excitation energies of the system. The time-dependence of the density is reflected in $\langle r^2 \rangle(t)$ (see equation (2.30)) and we can see the excitation energies in the spectrum of the turned-off run.

The spectrum of the generic-turned off run is shown in figure 2.13. In this graph we observe only one group of peaks, which have a similar constellation to those around $\omega = 0.95$ and $\omega = 0.2$ in the spectrum of the generic run: one peak of the exact calculation is on top of the 3d harmonic oscillator and the other exact peaks are lower.

The ALDA peak is roughly speaking in the middle of the exact peaks. The values are given in table 2.3.

The matching of the 3d harmonic oscillator peak with one of the peaks of the exact calculation is due to the close relation between the Hamiltonian of the center of mass system and the 3d harmonic oscillator, i.e. we can rewrite equation (2.5)

$$\begin{aligned} \hat{H}_R \phi(R) &= E_R \phi(R) && (2.35) \\ 2\hat{H}_R &= -\frac{1}{2}\nabla_R^2 + \frac{1}{2}4\Omega^2 R^2 && (2.36) \\ &= -\frac{1}{2}\nabla_R^2 + \frac{1}{2}\Omega_R^2 R^2 \,, \end{aligned}$$

where we use that $m_R = 2$ and introduce $\Omega_R = 2\Omega$. The eigenvalues for this 3d system with zero angular momentum are

$$\begin{aligned} 2E_R &= \Omega_R \,(2n_r + \frac{3}{2}) && (2.37) \\ \Rightarrow E_R &= \Omega \,(2n_r + \frac{3}{2}) && (2.38) \end{aligned}$$

These are exactly the energies of the 3d harmonic oscillator with the same force constant $k = \Omega^2$.

$k = 0.25\, \epsilon = 0.1$	3d harmonic oscillator	ALDA	exact		
$\omega = 0.75$	1.183	1.143	1.116	1.183	1.139

Table 2.3: This table shows the frequency peaks for the generic turned-off run, with $\omega = 0.75$. The last three columns show the exact peaks in the order of their height.

We can calculate the energies for Hooke's atom. They are the sum of the energy from the center of mass and the relative coordinate system. To get the center of mass energies, we just have to evaluate the 3d harmonic oscillator energies $\Omega\left(2n_r + \frac{3}{2}\right)$. The energies for the relative coordinate system can be calculated approximately by a matrix diagonalization of the Hamiltonian (2.6). This is done using a gaussian basis set [28]. Table 2.4 shows some of the eigenenergies of Hooke's atom. From this table we can

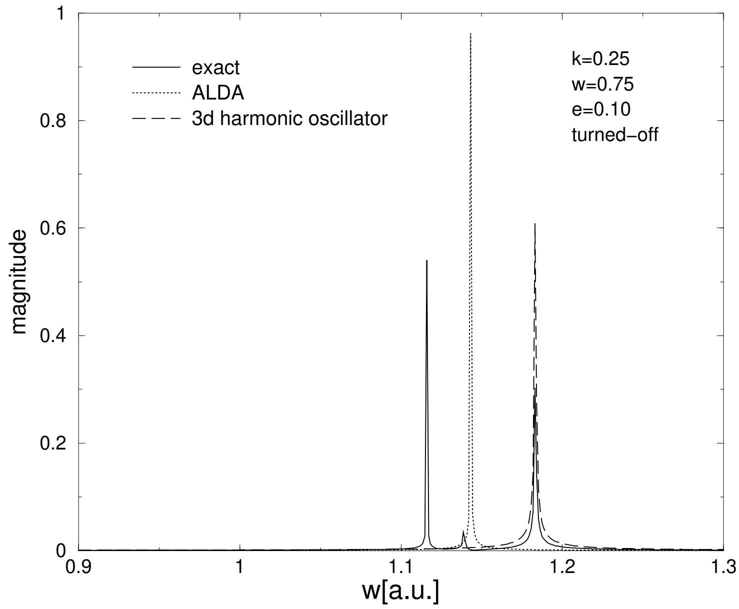

Figure 2.13: The plot shows the spectrum of $\langle r^2 \rangle(t)$ for the generic, where the force constant was kept constant after a half period. Before we Fourier transform, we cut off the time-evolution for $t \leq t_f$. Except for the peak positions, the graph looks similar to figures 2.9 and 2.10.

evaluate the different excitation energies. Note, that due to this type of basis set, we only need a small number of basis functions to get the lower eigenvalues. On the other hand the overlap matrix, which we have to invert is ill conditioned (due to specific basis set), so that we can trust these values only up to three digits. However, this is enough to demonstrate our analysis.

Now we are able to identify the peak positions with the excitation energies. For the generic turned-off run the exact peak on top of the harmonic peak corresponds to a transition from $(0,0) \to (0,1)$, where the first number describes the excitation level in the relative system and the second one in the center of mass system (n_u, n_R). This particular transition should have a peak at $\omega = 2\sqrt{0.25 + 0.1} \approx 1.18321$. This matches perfect with peak found in the $\langle r^2 \rangle$ spectrum at $\omega = 1.183$ (see table 2.3).
The second highest peak is explainable by the transition $(0,0) \to (1,0)$, which has the frequency $\omega = 1.12$. In the table 2.3, which lists the frequencies of the turned-off, we find $\omega = 1.116$. The third peak should be at $\omega = 1.14$. This again agrees

n_u	n_R	$k = 0.10$	$k = 0.25$	$k = 0.35$	$k = 1.00$
0	0	1.34	2.00	2.32	3.73
1	0	1.93	2.94	3.44	5.63
2	0	2.53	3.90	4.58	7.58
0	1	1.97	3.00	3.51	5.73
1	1	2.56	3.94	4.62	7.63
2	1	3.16	4.90	5.76	9.58
0	2	2.60	4.00	4.69	7.73
1	2	3.19	4.94	5.81	9.63
2	2	3.79	5.90	6.95	11.6

Table 2.4: The table shows the energy eigenvalues of Hooke's atom, for various values of the spring constant k, labeled by the quantum numbers n_u, n_R indicated on the left.

very well with the value found in the spectrum $\omega = 1.139$. It corresponds to the excitation $(1,1) \to (2,1)$. Note, that $(1,1) \to (1,2)$ yields the same transition frequency as $(0,0) \to (0,1)$. Transitions increasing the n_R quantum number are given by $\omega = 2j\sqrt{k(t_f)}$, where $j = n_R^{(1)} - n_R^{(2)}$, because of the uniform level spacing in the harmonic oscillator.

Note, that for the explanation of the *one* ALDA peak this expansion in eigenfunctions is not simple, because the Kohn-Sham potential is not static for $t \geq t_f$. The density is oscillating and therefore also the Kohn-Sham potential is oscillating. However we can assume that the oscillation of the density is very small, so that the ALDA Kohn-Sham potential is almost static.

In the ALDA (and harmonic oscillator) case, we are dealing with a single-particle picture with a one body-potential. The single-particle orbitals are products of a radial function with an angular one, because of the spherical symmetry of the potential. Since the Kohn-Sham system begins with both electrons having zero angular momentum and there is nothing in the Hamiltonian which can change angular momentum, the Kohn-Sham calculation can only make transitions to levels which also have $l = 0$. With the ϵ of the size in the generic run, we only make significant transitions to the first excited $l = 0$ level, changing the radial quantum number by 1; so we only expect to see one significant peak in the spectrum. The same holds for the 3d harmonic oscillator, as described earlier.

On the other hand in the exact run, we see two closely spaced peaks, one corresponding to an excitation in the center of mass coordinate R, and the other in the relative coordinate u. How can we reconcile this with the ALDA run? The answer lies in the angular momentum. The exact wave-function has total $L = 0$, with $l_u = 0$ and $l_R = 0$ being preserved along the time evolution. But if we go back to the r_1, r_2 coordinate system, rather than R, u, we find that a u-excitation is a linear combination of states of non-zero single-electron angular momentum, $l_i \neq 0$. Since the ALDA evolution preserves $l_1 = 0 = l_2$, it never reaches orbitals of non-zero l and so misses this excitation.

The multiple peaks in the exact calculation compared to only one frequency contribution for ALDA, cause a big difference in the behaviour of $\langle r^2 \rangle(t)$. Figure 2.12 shows the beating on top of the oscillating exact curve and a simple oscillating behaviour for the ALDA calculation and the 3d harmonic oscillator. These differences are also present in figure 2.14, where we plot $T_s(t)$ and $E_c(t)$ in the turned-off case.

We have explained the peak positions of the exact calculation and the harmonic oscillator for the turned-off run. To calculate the positions for the runs, where the perturbation lasts for the entire run is less trivial. From table 2.4 we get for $\bar{k} = 0.25$ the excitation energies:

$$
\begin{array}{ccccccc}
(0,0) & \rightarrow & (0,1) & \omega = 1.00 & (0.977) & [1.000] \\
(0,0) & \rightarrow & (1,0) & \omega = 0.94 & (0.920) & [0.940] \\
(1,1) & \rightarrow & (2,1) & \omega = 0.96 & (0.938) & [-]
\end{array}
$$

This seems not to match very well for generic run, where the values in parenthesis are from table 2.2, corresponding to $\epsilon = 0.1$. But at least the differences between these frequencies agree. However, for $\epsilon = 0.01$, the weak generic run we find a very good agreement (see square-brackets and table 2.2). So, when ϵ is small enough, treating the potential as if it were static at $\bar{k}$ seems to explain the peaks. Note, that for the weak generic run, the third exact peak does not occur, since the perturbation is too small to excite this state.

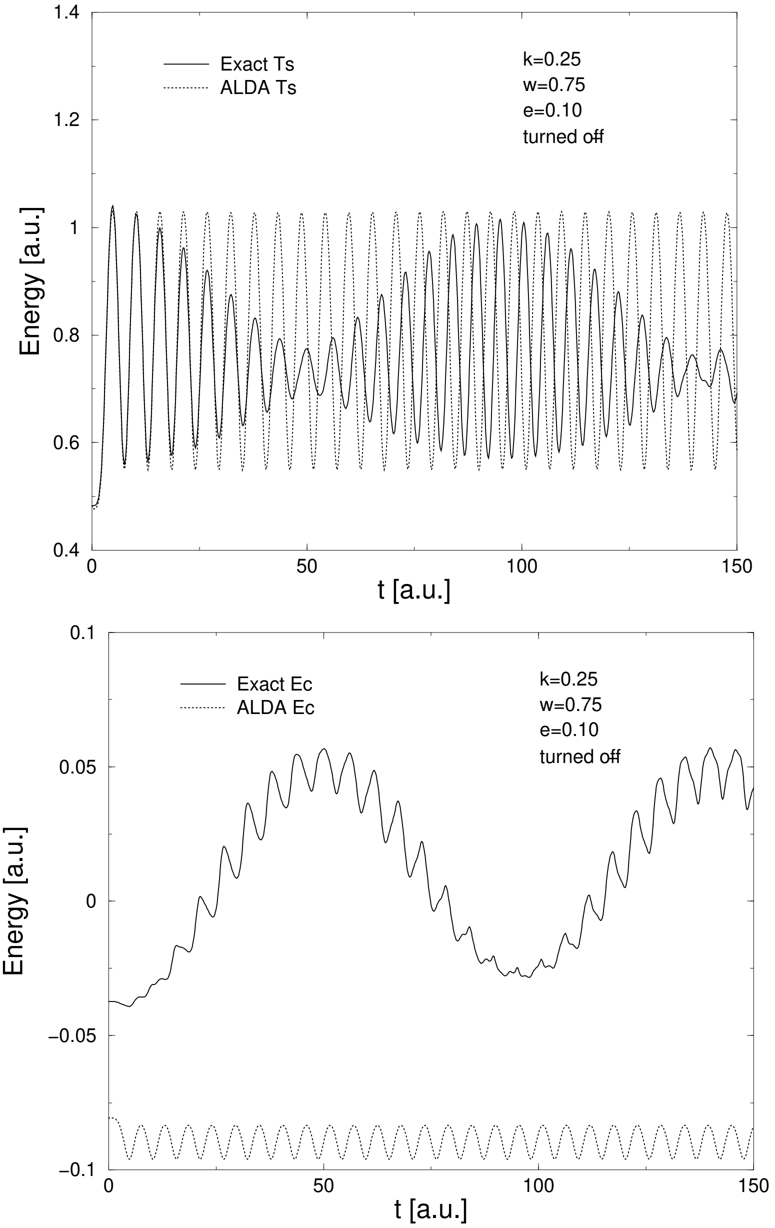

Figure 2.14: The graph shows the difference between the exact Kohn-Sham system, here the values for $E_c(t)$ and $T_s(t)$ and the approximated Kohn-Sham system (ALDA). The curves correspond to the generic run, where the perturbation was turned off after a half period. We can see a beating in the exact $T_s(t)$ curve, in contrast to the ALDA calculation.

Higher order contributions

In the generic run, we have also found peaks around $\omega = 0.2, 1.5, 1.70$, which are missing in the linear response equation (2.31) for $\langle r^2 \rangle$. We expect that for a smaller perturbation, given by the ratio of ϵ and $\bar{k}$, these higher order contributions become very small. For example, consider the weak generic run with $\epsilon = 0.01$ in figure 2.11: we notice that the group of peaks centered at $\omega = 0.2$ is very small. Also the oscillator peak that was at $\omega = 0.977$ for $\epsilon = 0.1$ has moved on top of the linear response peak $\omega = 1.000$.

We can explain these peaks for the 3d harmonic oscillator by calculating higher orders in time-dependent perturbation theory. What will happen in the evaluation of the higher order is, that the time-dependent terms consist of different sums of multiples of the perturbation frequency and multiples of $\sqrt{k(0)} = \sqrt{\bar{k} - \epsilon}$. Also, it will be necessary to expand this expression in ϵ. This explains why the peak of the 3d harmonic oscillator is not exactly at $\omega = 1.00$ in the generic spectrum.

For the interacting system these values are slightly different. But the principle is the same so we can predict the frequencies of the higher order contributions by adding and subtracting the peak positions for the two highest groups (from table 2.2):

$\bar{k} = 0.25$ $\omega = 0.75$ $\epsilon = 0.1$	subtracted	measured	added	measured
harmonic oscillator	0.227	0.227	1.727	1.730
ALDA	0.192	0.192	1.692	1.693
Exact 1	0.170	0.170	1.670	1.671
Exact 2	0.227	0.227	1.727	1.728
Exact 3	0.188	0.188	1.688	-

2.3 Conclusion

We have solved the time-evolution of the density for Hooke's atom by numerically solving the time-dependent Schrödinger equation. However this is only possible due to separability of Hooke's atom into two non-interacting systems: a 3d harmonic oscillator for center of mass system (2.5) and a 3d harmonic oscillator with an additional $\frac{1}{|\mathbf{u}|}$

potential for the relative coordinate system.

We compared the time evolution of this *exact* system with the ALDA density and found a good agreement for short times, but big differences for longer times and a complete different behaviour in runs, where we turned off the perturbation after a certain time t_f. Analyzing the Fourier spectrum of $\langle r^2 \rangle$ we found the reason for these differences. For all calculations in the generic run we found the highest peak at the perturbation frequency ω. However, the second highest set of peaks showed a different spectrum for the ALDA and the exact calculation: we found more peaks for the exact calculation than for ALDA.

We explained the peak positions for exact run in the turned-off case. The multiple peaks are due to transitions in the center of mass system (2.5) and the relative coordinate system (2.6). Assuming an (almost) static harmonic potential, this explanation predicted the peak positions for the weak generic run. We understand the ALDA peak, which is an excitation in a one-particle potential similar to the 3d harmonic oscillator. We explained that ALDA will miss some of the exact peaks due to the fact, that the Kohn-Sham-potential stays spherically symmetric. We expect that this will be a problem for ALDA for any spherically symmetric perturbation. This raises the question of how does the exact Kohn-Sham calculation manage to produce two peaks: after all, it is also a spherically-symmetric problem ? We suspect the answer lies in the careful analysis of memory effects, and the effects of phase-offsets, which are lost in the ALDA calculation.

It will also be necessary to explore, if our results can be linked to the calculation of atoms and molecules in a laser-field. The question is, whether ALDA will also miss excitations in these systems, although the details of our case are very different, in particular having spherical symmetry. More work is needed to understand this.

Appendix A

Linear response for the perturbed harmonic oscillator

Since the Hooke's atom is related to the harmonic oscillator, i.e. the center of mass Hamiltonian is a 3d harmonic oscillator, we can try to understand some of the time-dependent features of the system by exploring the harmonic oscillator within first order perturbation theory in ϵ.

We start with the 1d case and then easily generalize it to 3d later. Note, that the Hamiltonians for different times do not commute, so the time evolution operator has the form of a Dyson series.

The goal is to derive an expression for the density and for the expectation value of $< x^2 > (t)$ in first order in ϵ. The Hamiltonian for the perturbed 1D oscillator is given by

$$H = -\frac{1}{2}\left(\frac{\partial}{\partial x}\right)^2 + \frac{1}{2}x^2(\bar{k}-\epsilon) + \frac{\epsilon}{2}x^2(1-\cos(\omega t)) \tag{A.1}$$

$$H = H_0 + V(t). \tag{A.2}$$

The form of the Hamiltonian suggests the usage of the interaction picture. We want to start the system in the ground-state at $t = 0$, so the ground-state is the well known ground-state of a harmonic oscillator with $k(0) = \bar{k} - \epsilon$. The time evolution of this state is given by application of the time-evolution operator. To calculate the time evolution of the initial state we expand it using the orthonormal eigenfunctions of the harmonic oscillator, with $\Omega = \sqrt{k(0)}$ as natural frequency.

$$U_I(t,0) = 1 - i\int_0^t d\tau V_I(\tau) - i^2\int_0^t d\tau \int_0^\tau d\tau' \; V_I(\tau)V_I(\tau')U(\tau',0) \tag{A.3}$$

$$U_I = e^{iH_0 t} U e^{-iH_0 t} \tag{A.4}$$

$$|\Psi(t)\rangle = U|0\rangle = \sum_{k=0} \langle k|e^{-iH_0 t} U_I e^{iH_0 t}|0\rangle |k\rangle \tag{A.5}$$

$$= \sum_{k=0} e^{-i\underbrace{(E_k - E_0)}_{=k\,\Omega}t} \langle k|U_I|0\rangle|k\rangle \tag{A.6}$$

$$c_k(t) = \langle k|U_I|0\rangle = c_k^{(0)}(t) + c_k^{(1)}(t) + c_k^{(2)}(t) + \ldots \tag{A.7}$$

From (A.3) we know the expression for the coefficients $c_k^{(i)}(t)$

$$c_k^{(0)}(t) = \langle k|0\rangle = \delta_{k,0} \tag{A.8}$$

$$c_k^{(1)}(t) = -i\langle k|\int_0^t d\tau\ V_I(\tau)|0\rangle \tag{A.9}$$

$$= -\frac{i\epsilon}{2}\int_0^t d\tau\ e^{itk\,\Omega}\,(1-\cos(\omega t))\,\langle k|x^2|0\rangle \tag{A.10}$$

For the harmonic oscillator the position operator can be expressed as a sum of a creation and an annihilation operator, so that

$$\langle k|x^2|0\rangle = \frac{1}{2\Omega}\langle k|a^2 + a^{\dagger^2} + 1 + 2a^\dagger a|0\rangle \tag{A.11}$$

$$= \frac{1}{2\Omega}\left(\delta_{k,2}\sqrt{2} + \delta_{k,0}\right). \tag{A.12}$$

So we will have only two contributions for first order coefficient

$$c_0^{(1)}(t) = -\frac{i\epsilon}{4\Omega}\left(t - \frac{\sin(\omega t)}{\omega}\right) \tag{A.13}$$

$$c_2^{(1)}(t) = -\frac{\epsilon\sqrt{2}}{4\Omega}\left[\frac{e^{i\,2\Omega t}-1}{2\Omega} - \frac{e^{i(2\Omega+\omega)\,t}-1}{2(2\Omega+\omega)} - \frac{e^{i(2\Omega-\omega)\,t}-1}{2(2\Omega-\omega)}\right] \tag{A.14}$$

So the explicit form of the time evolution of the perturbed oscillator wave-function is

$$\begin{aligned}|\Psi(t)\rangle = \ & \left(1 - \frac{i\epsilon}{4\Omega}\left(t - \frac{\sin(\omega t)}{\omega}\right)\right)|0\rangle \\ & -e^{it2\Omega}\frac{\epsilon\sqrt{2}}{4\Omega}\left[\frac{e^{i\,2\Omega t}-1}{2\Omega} - \frac{e^{i(2\Omega+\omega)\,t}-1}{2(2\Omega+\omega)} - \frac{e^{i(2\Omega-\omega)\,t}-1}{2(2\Omega-\omega)}\right]|2\rangle\end{aligned} \tag{A.15}$$

A good measure for the time-dependent behaviour of the density is the expectation value $\langle x^2\rangle(t)$, which is the variance or spread of the wave-function. Again, the position operator can be expressed in terms of creation and annihilation operators

$$\langle\Psi(t)|x^2|\Psi(t)\rangle = \frac{1}{2\Omega}\langle a^2 + a^{\dagger^2} + 1 + 2a^\dagger a\rangle \tag{A.16}$$

$$\langle 0|x^2|0\rangle = \frac{1}{2\Omega} \tag{A.17}$$

$$\langle 0|x^2|2\rangle = \frac{1}{2\Omega}\sqrt{2} \tag{A.18}$$

$$\langle 2|x^2|0\rangle = \frac{1}{2\Omega}\sqrt{2} \tag{A.19}$$

$$\langle 2|x^2|2\rangle = \frac{5}{2\Omega} \tag{A.20}$$

(A.21)

Using these expectation values the calculation in first order of ϵ yields

$$\langle\, x^2\,\rangle \;=\; \frac{1}{2\sqrt{\bar{k}}} + \frac{\epsilon}{\sqrt{\bar{k}}\,(4\bar{k}-\omega^2)}\cos\omega t - \frac{\epsilon\,\omega^2}{4\bar{k}^{3/2}\,(4\bar{k}-\omega^2)}\cos\left(2\sqrt{\bar{k}}t\right) \qquad \text{(A.22)}$$

where we have expanded $\Omega = \sqrt{\bar{k}-\epsilon}$ to first order in ϵ and dropped all the higher order terms from (A.15). The generalization to 3D is easy, because we only deal with a spherical symmetric problem at all times. Therefore

$$\langle\, r^2\,\rangle \;=\; \langle\, x^2+y^2+z^2\,\rangle = 3\langle\, x^2\,\rangle \qquad \text{(A.23)}$$

For $\omega = 2\Omega$ the first order coefficient (A.13) has a singularity. For this resonance case we find

$$\begin{aligned}\langle\, x^2\,\rangle = \;& \frac{1}{2\sqrt{\bar{k}}} + \qquad \text{(A.24)}\\ & \frac{\epsilon}{4\bar{k}}\left(\frac{\cos\left(2\sqrt{\bar{k}}t\right)}{\sqrt{\bar{k}}} + t\sin\left(2\sqrt{\bar{k}}t\right) - \frac{\cos\left(2\sqrt{\bar{k}}t\right)-\cos\left(\omega t\right)}{2\sqrt{\bar{k}}+\omega}\right).\end{aligned}$$

Appendix B

Imaginary time propagation (ITP)

We want to start the ALDA time evolution in its ground-state, therefore we have to do a self-consistent calculation as described in section 1.1.2. Since we have already a time-propagation method, i.e. the Crank-Nicolson (CN) algorithm, it turns out that an imaginary time propagation (ITP) method is very convenient to obtain the ground-state. So we just use the CN method with an imaginary time step: $\tilde{dt} = -idt$.

To see how ITP works we expand the "guessed" initial state in the (unknown) eigenfunctions of the system and apply the infinitesimal time evolution operator

$$
\begin{aligned}
U(dt,0)|\Phi\rangle &= c_0(1 - iH\tilde{dt})|0\rangle + \ldots + c_{k_{max}}(1 - iH\tilde{dt})|k_{max}\rangle && \text{(B.1)} \\
&= c_0 \underbrace{(1 - E_0 dt)}_{\xi_0} |0\rangle + \ldots + c_{k_{max}} \underbrace{(1 - E_{k_{max}} dt)}_{\xi_{k_{max}}} |k_{max}\rangle && \text{(B.2)}
\end{aligned}
$$

Note, that since we are dealing with a finite grid, there is a maximum eigenvalue $E_{k_{max}}$ and eigenfunction $|k_{max}\rangle$. In our case the eigenvalues are all positive $0 < E_0 < \ldots < E_{k_{max}}$, therefore the factors ξ_j decrease with increasing j (given a small enough dt). Applying the infinitesimal time evolution operator n times shows that the eigenfunction with the smallest prefactor ξ_j "dies" the fastest. Therefore the "guessed" initial state is "purified" from the excited states and the ground-state $|0\rangle$ remains. However, the norm is not conserved, so it is important to renormalize the wave-function after each step (or a certain number of steps).

In equation (B.1) the form of the prefactors have the form of an explicit propagation scheme. For the CN method the equation is

$$
\begin{aligned}
U(dt,0)|\Phi\rangle &= c_0 \frac{1 - \frac{1}{2}Hdt}{1 + \frac{1}{2}Hdt}|0\rangle + \ldots + c_{k_{max}} \frac{1 - \frac{1}{2}Hdt}{1 + \frac{1}{2}Hdt}|k_{max}\rangle && \text{(B.3)} \\
&\approx c_0(1 - \frac{1}{2}E_0 dt)^2|0\rangle + \ldots + c_{k_{max}}(1 - \frac{1}{2}E_{k_{max}} dt)^2|k_{max}\rangle && \text{(B.4)}
\end{aligned}
$$

using the Taylor expansion

$$
\frac{1}{1+x} = 1 - x + O(x^2). \tag{B.5}
$$

There are no significant changes compared to the explicit scheme, the time step dt remains important.

Note, if the time step is too large the iteration will converge against the highest possible eigenvalue on the grid. Since the size of the grid determines the largest eigenvalue, the time step depends also on the grid size, i.e. we have to use a smaller time step for a finer grid.

A question that remains is, how long do we have to do the iteration ?

In our work we calculate the total energy and compare it to the value it had a certain number of imaginary time steps before. If the difference is smaller than a certain threshold value, we stop the (imaginary) time propagation. The success of the ITP is shown in figures B.1. The oscillation of the $\langle r^2(t) \rangle^{ALDA}$ curve without ITP around the other ALDA curve is due to the mixing of higher eigenfunctions. In other words the system is not really in its ground-state, but in a superposition of states, basically the ground-state and the first excited state. In this run the perturbation frequency was $\omega = 0.01$, which is clearly in the adiabatic regime. So the system finds itself always in the ground-state. The perturbation was turned off after a half period.

If we examine the top-graph carefully, we notice that the frequency of the oscillation changes with time. This happens because the energy difference between ground-state and first excited state changes proportional to the natural frequency $\Omega = \sqrt{k(t)}$, which is time-dependent.

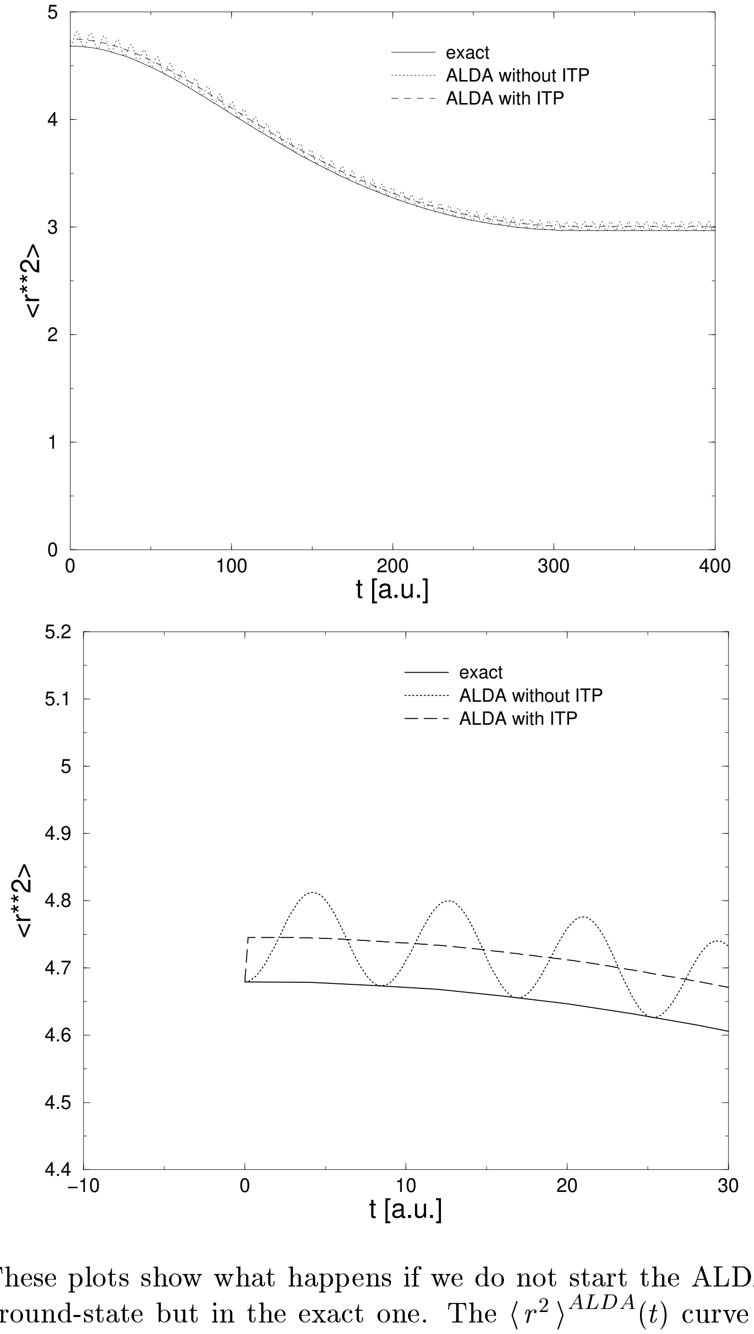

Figure B.1: These plots show what happens if we do not start the ALDA calculation in the LDA ground-state but in the exact one. The $\langle r^2 \rangle^{ALDA}(t)$ curve without ITP oscillates around the curve, where the calculation was started in the LDA ground-state. The oscillation is mainly due to the first excitation. The zoomed graph shows that the value of $\langle r^2 \rangle^{ALDA}(0)$ jumps due to the ITP (dashed line). These effects are demonstrated for a perturbation frequency, which is within the adiabatic regime, so the system finds itself in a ground-state for all times.

References

[1] R.M. Dreizler and E.K.U. Gross. *Density functional theory : An approach to the quantum many-body problem.* Springer, 1990.

[2] P. Hohenberg and W. Kohn. Inhomogeneous electron gas. *Phys. Rev.*, 136(3B):864, November 1964.

[3] W. Kohn and L.J. Sham. Self-consistent equations including exchange and correlation effects. *Phys. Rev.*, 140(4A):1133, November 1965.

[4] M. Ernzerhof, J.P. Perdew, and K. Burke. Density functionals: Where do they come from ? Why do they work ? in: Density Functional Theory, ed. R. Nalewajski, 1996.

[5] A.D. Becke. Density-functional exchange-energy approximation with correct asymptotic behavior. *Phys. Rev. A*, 38:3098, 1998.

[6] F. Bloch. *Z. Physik*, 81:363, 1933.

[7] A. Zangwill and P. Soven. Density-functional approach to local-field effects in finite systems: Photoabsorption in the rare gases. *Phys. Rev. A*, 21(5):1561, May 1980.

[8] V. Peuckert. *J. Phys. Chem.*, 11:4945, 1978.

[9] B.M. Deb and S.K. Ghosh. *J. Chem. Phys.*, 77:342, 1982.

[10] B.M. Deb and S.K. Ghosh. *J. Chem. Phys.*, 71:295, 1982.

[11] B.M. Deb and S.K. Ghosh. *Theoret. Chem. Acc.*, 62:209, 1983.

[12] B.M. Deb and S.K. Ghosh. *J. Mol. Struct.*, 103:163, 1983.

[13] L.J. Bartolotti. *Phys. Rev. A*, 24:1661, 1981.

[14] L.J Bartolotti. *Phys. Rev. A*, 26:2243, 1982.

[15] L.J Bartolotti. *J. Chem. Phys.*, 80:5687, 1984.

[16] L.J Bartolotti. *Phys.Rev. A*, 36:4492, 1987.

[17] E. Runge and E.K.U. Gross. Density-functional theory for time-dependent systems. *Phys. Rev. Lett.*, 52:997–1000, 1984.

[18] R. van Leeuwen. Mapping from densities to potentials in time-dependent density-functional theory. *Phys. Rev. Lett.*, 82:3863, 1999.

[19] N.T. Maitra and K. Burke. Demonstration of initial-state dependence in time-dependent density-functional theory. *Phys. Rev. A*, 63:042501, 2001.

[20] E.K.U. Gross, E. Runge, and O. Heinonen. *Many-particle theory.* Adam Hilger, Bristol, 1991.

[21] G. Vignale and W. Kohn. Current-dependent exchange-correlation potential for dynamical linear response theory. *Phys. Rev. Lett.*, 77:2037, 1996.

[22] J.F. Dobson, M. Bünner, and E.K.U. Gross. Time-dependent density functional theory beyond linear response: An exchange-correlation potential with memory. *Phys. Rev. Lett.*, 79:1905, 1997.

[23] G. Vignale, C.A. Ullrich, and S. Conti. Time-dependent density functional theory beyond the adiabatic local density approximation. *Phys. Rev. Lett.*, 79:4878, 1997.

[24] E.K.U Gross, J.F. Dobson, and M. Petersilka. Density functional theory of time-dependent phenomena. *Topics in current chemistry*, 181:81–172, 1996.

[25] L. Brey, N.F. Johnson, and B.I. Halperin. *Phys. Rev. B*, 40:10647, 1989.

[26] N.T.Maitra, K. Burke, and C. Woodward. Memory effects in time-dependent density functional theory. submitted (2001).

[27] M. Petersilka, U.J. Gossmann, and E.K.U. Gross. Excitation energies from time-dependent density functional theory. *Phys. Rev. Lett.*, 76(8):1212, February 1996.

[28] H. Appel. Oscillator strength from time-dependent density functional theory. Master's thesis, Rutgers, New Brunswick, New Brunswick, NJ, October 1999.

[29] S. J. A. van Gisbergen, A. Rosa, G. Ricciardi, and E. J. Baerends. Time-dependent density functional calculations on the electronic absorption spectrum of free base porphin. *J. Chem. Phys.*, 111(6):2499, 1999.

[30] R.E. Stratmann, G.E. Scuseria, and M.J. Frisch. An efficient implementation of time-dependent density-functional theory for the calculation of excitation energies of large molecules. *J. Chem. Phys.*, 109(19):8218, 1998.

[31] H.H. Heinze, A. Görling, and N. Rösch. An efficient method for calculating molecular excitation energies by time-dependent density-functional theory. *J. Chem. Phys.*, 113(6):2088, August 2000.

[32] D. Sundholm. Density functional theory calculation of the visible spectrum of chlorophyll α. *Chem. Phys. Lett.*, 302:480, 1999.

[33] K. Tatarczyk, A. Schindlmayr, and M. Scheffler. Exchange-correlation kernels for excited states in solids. *Phys. Rev. B*, 63:235106, June 2001.

[34] S.J.A. Gisbergen et al. A density functional theory study of frequency dependent polarizibility and van der Waals dispersion coefficients for polyatomic molecules. *J. Chem. Phys.*, 103(21):9347, 1995.

[35] G.T. Velde et al. Chemistry with adf. *J. Comp. Chem.*, 22(9):931–967, July 2001.

[36] S.J.A. Gisbergen et al. Excitation energies for transition metal compounds from time-dependent density functional theory. Applications to MnO_4^-, $Ni(CO)_4$, and $Mn_2(CO)_10$. *J. Phys. Chem. A*, 103(34):6835, 1999.

[37] Lerme et al. Optical properties of gold metal clusters: A time-dependent local-density-approximation investigation. *Euro. Phys. J. D*, 4(1):95–108, October 1998.

[38] K. Yabana and G.F. Bertsch. Optical response of small silver clusters. *Phys. Rev. A*, 60:3809, August 1999.

[39] K. Yabana and G.F. Bertsch. Applications of the time-dependent local density approximation to optical activity. *Phys. Rev. A*, 60(2):1271, 1999.

[40] Rubio et al. Ab initio photoabsorption spectra and structures of small semiconductor and metal clusters. *J. Chem. Phys.*, 77(2), 1996.

[41] I. Vasiliev, S. Ögüt, and J.R. Chelikowsky. Ab initio spectra and optical gaps in nanocrystalline silicon. *Phys. Rev. Lett.*, 86(9):1813, February 2001.

[42] C.A. Ullrich and E.K.U. Gross. Many-electron atoms in strong femto-second laser pulses: A density-functional study. *Comm. At. Mol. Phys.*, 33:211, 1997.

[43] D. Bauer and F. Ceccherini. Time-dependent density functional theory applied to nonsequential multiple ionization of Ne at 800 nm. *Optics Express*, 8(7):377, March 2001.

[44] M. Petersilka and E.K.U. Gross. Strong-field double ionization of helium: A density functional perspective. *Laser Physics*, 9:105, 1999.

[45] Reinhard et al. Frequencies, times, and forces in the dynamics of Na clusters. *Euro. Phys. J. D*, 9(1-4):111–117, December 1999.

[46] K. Burke, F.G. Cruz, and K. C. Lam. Unambiguous exchange-correlation energy density for hooke's atom. *Int. J. Quantum Chem.*, 70:583, 1998.

[47] K. C. Lam, F.G. Cruz, and K. Burke. Virial exchange-correlation energy density in hooke's atom. *Int. J. Quantum Chem.*, 69:533, 1998.

[48] R.M.G. Garcia-Castelan, W.S. Choe, and Y.C. Lee. Correlation energies for two interacting electrons in a harmonic dot. *Phys. Rev. B*, 57(16):9792, April 1998.

[49] M. Taut. Two electrons in an external oscillator potential: Particular analytic solutions of a coulomb correlation problem. *Phys. Rev. A*, 48(5):3561, 1993.

[50] S. Kais, D.R. Herschbach, and R.D. Levine. Dimensional scaling as a symmetry operation. *J.Chem. Phys.*, 91:7791, 1989.

[51] P.M. Laufer and J.B. Krieger. Test of density-functional approximations in an exactly soluble model. *Phys. Rev. A*, 33(3):1480, 1986.

[52] Zhixin Qian and Viraht Sahni. Physics of transformation from Schrödinger theory to Kohn-Sham density-functional theory: Application to an exactly solvable model. *Phys. Rev. A*, 57(4):2527, April 1998.

[53] A.H. Nayfeh and D.T. Mook. *Nonlinear Oscillations.* Wiley, New York, 1979.

[54] J.F. Dobson. Harmonic potential theorem: Implications for approximate many-body theories. *Phys. Rev. Lett.*, 73:2244, 1994.

[55] P. Hessler, J. Park, and K. Burke. Several theorems in time-dependent density functional theory. *Phys. Rev. Lett.*, 83:5184, 1999.

[56] P. Hessler, N.T. Maitra, and K. Burke. Dynamic effects in time-dependent density functional theory. *in preparation*, 2000.

[57] A.L. Garcia. *Numerical Methods for Physics*. Prentice Hall, Englewood Cliffs, New Jersey, 1994.

[58] W.H. Press, B.P. Flannery, S.A. Teukolsky, and W.T. Vetterling. *Numerical Recipes*. Cambridge University Press, Cambridge, UK, 1994.

[59] J. P. Perdew and Y. Wang. Accurate and simple analytic representation of the electron-gas correlation energy. *Phys. Rev. B*, 45:13244, 1992.